Finite element solution of hyperbolic equations II. Two dimensional case

Vittorio Selmin

INRIA

UNITÉ DE RECHERCHE
INRIA-SOPHIA ANTIPOLIS

Institut National
de Recherche
en Informatique
et en Automatique

Domaine de Voluceau
Rocquencourt
BP 105
78153 Le Chesnay Cedex
France
Tél. (1) 39 63 55 11

Rapports de Recherche

N° 708

FINITE ELEMENT SOLUTION OF HYPERBOLIC EQUATIONS II. TWO DIMENSIONAL CASE

Vittorio SELMIN

JUILLET 1987

FINITE ELEMENT SOLUTION OF HYPERBOLIC EQUATIONS II. TWO DIMENSIONAL CASE

RESOLUTION D'EQUATIONS HYPERBOLIQUES PAR UNE METHODE D'ELEMENTS FINIS II. LE CAS BIDIMENSIONNEL

Vittorio SELMIN

INRIA Sophia-Antipolis
Avenue Emile Hughes
(Anc. Route des Lucioles)
Sophia Antipolis
06565 VALBONNE

Abstract

We compare a number of methods which intend to combine the advantages of a monotone scheme, which produces no "ripples" near discontinuities, together with those of a second-order one. These two schemes are formulated within the framework of the Taylor-Galerkin finite element method. We have tested artificial viscosity methods, TVD methods and FCT methods. Numerical results of the computation of hypersonic flows around a blunt body are presented.

Résumé

On compare différentes méthodes qui essayent de combiner les avantages d'un schéma monotone, qui ne produit pas d'oscillations près des discontinuités, avec ceux d'un schéma précis au second ordre. Ces deux schémas sont construits en utilisant la méthode Taylor-Galerkin des éléments finis. On a testé des méthodes de viscosité artificielle, des méthodes TVD et des méthodes FCT. Des exemples numériques concernant la résolution d' écoulements hypersoniques autour d'un corps arrondis sont présentés.

I. Introduction

In the following, we extend to the two-dimensional case some non oscillatory shock-capturing schemes described in a previous report [1] concerning the solution of one-dimensional hyperbolic problems. We compare a number of methods which intend to combine the advantages of a monotone scheme, which produces no 'ripples' near discontinuities, with those of a second-order one. These two schemes are formulated within the framework of the Taylor-Galerkin finite element method[2]. The difference between the two schemes is a discretization of a Laplacian operator which uses the dissipative effect of the well-known mass matrix operator of the finite element formulation. The main idea of this paper is that, using P^1 triangular elements, the dissipative operator constructed on an element can be distributed over its sides which will be subsequently named segments. Thus, we can replace the element contributions to the discretization of the dissipative operator by segment contributions and use the one-dimensional character of the latter to generalize one-dimensional methods described in [1].

An outline of the report follows. In section II, we present the Euler equations and a very brief description of the finite element spatial dicretization; then, in section III, we discuss first- and second-order schemes formulated within the framework of the finite element methods of Taylor-Galerkin type. In section IV, we describe the artificial viscosity method, the Total Variation Diminishing (TVD) concept and the Flux Corrected Transport (FCT) technique, respectively. Finally, in section V, numerical results of the computation of hypersonic flows around a blunt body are presented.

II. Mathematical modelling

1. Governing equations

The conservative form of the Euler equations in the two-dimensional space is given by :

$$\frac{\partial U}{\partial t} + \frac{\partial F(U)}{\partial x} + \frac{\partial G(U)}{\partial y} = 0 \tag{1}$$

in which

$$U = \begin{pmatrix} \rho \\ \rho u \\ \rho v \\ e \end{pmatrix} , \; F = \begin{pmatrix} \rho u \\ \rho u^2 + p \\ \rho uv \\ u(e+p) \end{pmatrix} , \; G = \begin{pmatrix} \rho v \\ \rho uv \\ \rho v^2 + p \\ v(e+p) \end{pmatrix}$$

where ρ is the density, $\overrightarrow{w} = (u, v)$ is the velocity vector, e is the total energy per unit volume and p is the pressure. We assume that the fluid satisfies the perfect gas law :

$$p = (\gamma - 1)(e - \rho \frac{u^2 + v^2}{2})$$

where γ is the ratio of specific heats ($\gamma = 1.4$ for air).
Let A and B denote the Jacobian matrix $\partial F(U)/\partial U$ and $\partial G(U)/\partial U$ whose eigenvalues are

$$(a^1, a^2, a^3, a^4) = (u - c, u, u, u + c)$$

and

$$(b^1, b^2, b^3, b^4) = (v - c, v, v, v + c)$$

respectively, where $c = \sqrt{\gamma p/\rho}$ is the speed of sound.
Eq.(1) can be written in the non conservative form :

$$\frac{\partial U}{\partial t} + A(U)\frac{\partial U}{\partial x} + B(U)\frac{\partial U}{\partial y} = 0$$

2. Finite element approximation

In order to discretize the continuous problem, the flow region is imbedded in a bounded polygonal domain Ω whose boundary is denoted by Γ. A triangulation T with charateristic mesh spacing h is introduced on Ω. The vertices of the triangles define a set of computational nodes, S , where the numerical solution of (1) is to be computed. For each node S_i, a piecewise linear basis function $N_i(x,y)$ of support Ω_i is introduced where Ω_i is the union of the elements T_i^l that possess the node S_i as vertex. It is a first degree polynomial on each element T_i^l of T which takes the value 0 for all the nodes except for S_i where $N_i(x_i,y_i) = 1$.

Any scalar function $u(x,y)$ on Ω can be approximated by :

$$u^h(x,y) = \sum_i N_i(x,y)\ u(x_i,y_i)$$

where the sum is over all the nodes of S. In practice, for a given (x,y), the sum involves only three terms :

$$u^h(x,y) = \sum_{i=1}^{3} N_i(x,y)\ u(x_i,y_i) \quad ,$$

namely those corresponding to the basis functions N_i associated with the vertices of the triangle containing (x,y).

III. First- and second-order finite element schemes

1. Second-order scheme

The Eq.(1) is discretized in time as in the classical Lax-Wendroff scheme [3] or in the Taylor-Galerkin scheme of second-order accuracy in time[4] :

$$\frac{U^{n+1}-U^n}{\Delta t} = -(\frac{\partial F^n}{\partial x}+\frac{\partial G^n}{\partial y}) + \frac{\Delta t}{2}\frac{\partial}{\partial x}[A^n(\frac{\partial F^n}{\partial x}+\frac{\partial G^n}{\partial y})] + \frac{\Delta t}{2}\frac{\partial}{\partial y}[B^n(\frac{\partial F^n}{\partial x}+\frac{\partial G^n}{\partial y})] \tag{2}$$

in which $U^n = U(x,y,t^n)$, $F^n = F(U^n)$ and $G^n = G(U^n)$, where subscript n is the time level so that $t^n = n\Delta t$ and Δt is the time increment .
To introduce a spatial approximation by means of the finite element method, Eq.(2) must be recast in a weak form according to the standard weighted residual formulation which gives, after integrating by parts the second-order terms,

$$\int_\Omega w\,\frac{U^{n+1}-U^n}{\Delta t}d\Omega = RH\Omega^n + RH\Gamma^n \tag{3}$$

where

$$RH\Omega^n = \int_\Omega \{\frac{\partial w}{\partial x}[F^n - \frac{\Delta t}{2}A^n(\frac{\partial F^n}{\partial x}+\frac{\partial G^n}{\partial y})] + \frac{\partial w}{\partial y}[G^n - \frac{\Delta t}{2}B^n(\frac{\partial F^n}{\partial x}+\frac{\partial G^n}{\partial y})]\}d\Omega$$

and

$$RH\Gamma^n = \int_\Gamma w\{\kappa_x[-F^n+\frac{\Delta t}{2}A^n(\frac{\partial F^n}{\partial x}+\frac{\partial G^n}{\partial y})]+\kappa_y[-G^n+\frac{\Delta t}{2}B^n(\frac{\partial F^n}{\partial x}+\frac{\partial G^n}{\partial y})]\}d\Gamma$$

$\overrightarrow{\kappa} = (\kappa_x, \kappa_y)$ is the outward unit vector normal to Γ .
The spatial approximation of (2) at node S_i is performed according to the standard Galerkin finite element method for which the weighting function w is chosen as the basis function $N_i(x,y)$.
The equation thus obtained can be written in the form

$$\int_\Omega N_i\,U^{n+1}d\Omega = \int_\Omega N_i\,U^n d\Omega + RH_i^n \tag{4}$$

where $RH_i^n = \Delta t(RH\Omega_i^n + RH\Gamma_i^n)$.
Since the left-hand side of Eq.(4) involves values of the variables for all the nodes lying in Ω_i, the resulting system is, by nature, implicit.

2. First-order scheme

If the consistent mass matrix is diagonalized(or lumped), i.e., if one introduces the approximation

$$\int_\Omega N_i\ U^{n+1} d\Omega \rightarrow \int_\Omega N_i\ U_i^{n+1} d\Omega$$

in the left-hand side of Eq.(4) (but not in the right-hand side), the following first-order accurate scheme is obtained

$$\int_\Omega N_i\ U_i^{n+1} d\Omega = \int_\Omega N_i\ U^n d\Omega + RH_i^n \tag{5}$$

where $U_i^n = U(x_i, y_i, n\Delta t)$.
This scheme can be interpreted as a second-order approximation of a parabolic equation of the form

$$\frac{\partial U}{\partial t} + \frac{\partial F}{\partial x} + \frac{\partial G}{\partial y} = \frac{h^2}{6\Delta t}\ \Delta U$$

where Δ is a laplacian operator.
The first-order scheme can also be implemented by means of a splitting-up procedure. In fact, Eq.(5) is equivalent to the following two-step scheme :

$$\begin{cases} \int_\Omega N_i\ U^{n+\frac{1}{2}} d\Omega = \int_\Omega N_i\ U^n d\Omega + RH_i^n \\ \int_\Omega N_i\ U_i^{n+1} d\Omega = \int_\Omega N_i\ U^{n+\frac{1}{2}} d\Omega \end{cases} \tag{6}$$

Notice that the diffusion step introduces only a real multiplicative coefficient into the amplification factor with respect to that associated to Eq.(4) and do not disturb the phases [1].

3. Structure of the dissipative effect of the first-order scheme

3.1. *Element contribution*

The dissipative operator of the first-order scheme at node S_i can be written as

$$D_i U_i = \int_{\Omega_i} N_i\ (U - U_i) d\Omega \tag{7}$$

This term is composed, in fact, of the contribution of each element T_i^l that possesses the node S_i as vertex :

$$D_i U_i = \sum_l D_i^l\ U_i \tag{8}$$

where $D_i^l\ U_i = \int_{T_i^l} N_i (U - U_i) d\Omega.$

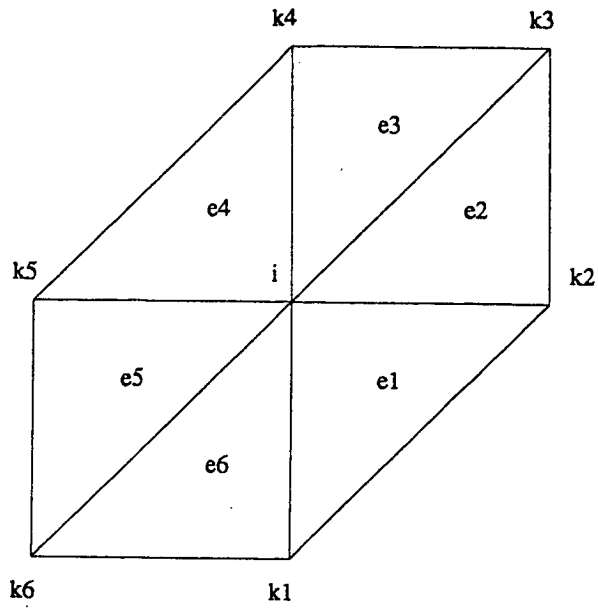

Fig.1: Elements and segments around the node S_i .

3.2. *Segment contribution*

It is interesting to distribute the contribution of the element over the segments which join two adjacent nodes. Denoting by S_{k1} and S_{k2} the two other nodes of the element T_i^l, $D_i^l\ U_i$ can be written as :

$$D_i^l\ U_i = K_{ik1}^l(U_{k1} - U_i) + K_{ik2}^l(U_{k2} - U_i)$$

where $K_{ij}^l = \int_{T_i^l} N_i N_j d\Omega$.

Using this decomposition, Eq.(8) becomes :

$$D_i U_i = \sum_k K_{ik}(U_k - U_i) \tag{9}$$

where the sum is over all the nodes surrounding the node S_i and $K_{ik} = \sum_l K_{ik}^l$.

The decomposition of the dissipative operator by segments is used subsquently to generalize some one-dimensional second-order non oscillatory schemes [1] to the multidimensional case.

4. First-order scheme with modulated dissipation

The dissipation term (9) of the first-order scheme can be modulated by introducing a parameter d, $0 \leq d \leq 1$. Two different schemes are obtained depending on whether the one-step or two-step form of the monotone scheme is started from.

4.1. *One-step scheme with modulated dissipation*

$$\int_\Omega N_i \, U_i^{n+1} d\Omega = \int_\Omega N_i \, U_i^n d\Omega + RH_i^n + \sum_k d_{ik} K_{ik} (U_k^n - U_i^n) \tag{10}$$

In the case $d_{ik} = 0$, we obtain a Lax-Wendroff type scheme [4].

4.2. *Two-step scheme with modulated dissipation*

$$\begin{cases} \int_\Omega N_i \, U^{n+\frac{1}{2}} d\Omega = \int_\Omega N_i \, U^n d\Omega + RH_i^n \\ \int_\Omega N_i \, U_i^{n+1} d\Omega = \int_\Omega N_i \, U_i^{n+\frac{1}{2}} d\Omega + \sum_k d_{ik} K_{ik} (U_k^{n+\frac{1}{2}} - U_i^{n+\frac{1}{2}}) \end{cases} \tag{11}$$

In the case $d_{ik} = 0$, scheme (4) is obtained.

For the last two schemes, it can be useful to introduce the artificial viscosity operator

$$AD_i \, U_i = \sum_k D_{ik} \, U_i \tag{12}$$

where

$$D_{ik} \, U_i = d_{ik} K_{ik} (U_k - U_i) \tag{13}$$

IV. Numerical methods

1. Artificial viscosity method

The solution obtained with second-order schemes suffers from dispersive "ripples" particularly near discontinuities whereas the first-order scheme produces no ripples but suffer from excessive numerical diffusion. The concept of artificial viscosity consists in modulating the effect of this dissipation by means of the parameter d. This coefficient may be $O(1)$ near discontinuities and $O(h^2)$ in the regions where the flow is "regular" to preserve the accuracy of the second-order scheme. Hence, at the discontinuities, the scheme is essentially the non oscillatory first-order scheme. Of course, the parameter d must be a function of a sensor which recognizes discontinuities in the flow.

An effective sensor of the presence of the shock wave can be constructed by taking the second derivative of the pressure. Denoting by S_i and S_k the nodes which delimit the segment $\{ik\}$, we introduce the quantity

$$d_i = |\frac{p_k - 2p_i + p_{i*}}{p_k + 2p_i + p_{i*}}| \tag{14}$$

where

$$p_{i*} = p_k - 2\overrightarrow{\nabla} p_i \cdot \overrightarrow{\eta} \tag{15}$$

is the pressure extrapolated in the direction $\overrightarrow{\eta} = (x_k - x_i \ ; \ y_k - y_i)$ from the node S_i and $\overrightarrow{\nabla} p_i$ is the gradient of the pressure calculated at this node. Similarly, we define

$$d_k = |\frac{p_{k*} - 2p_k + p_i}{p_{k*} + 2p_k + p_i}| \tag{16}$$

where

$$p_{k*} = p_i + 2\overrightarrow{\nabla} p_k \cdot \overrightarrow{\eta} \tag{17}$$

Note that d_i and d_k appear to be evaluations, at nodes S_i and S_k , of a non dimensional second order derivative of the pressure in the direction $\overrightarrow{\eta}$.
Finally, the coefficient of artificial viscosity d_{ik} is expressed as

$$d_{ik} = \chi \ max(d_i, d_k) \tag{18}$$

where χ is an adjustable parameter. Here the quantity d_{ik} is maximum on both sides of a shock but becomes zero inside. The disadvantage of the artificial viscosity methods lies in that they introduce an adjustable parameter whose value is not always simple to determine. In the next sections parameter free methods will be discussed.

2. Symmetric TVD methods

We can obtain second-order TVD scheme (without any adjustable parameter) using the following strategy :

i) Locate the place where the second-order accurate scheme produce oscillations
ii) Insert there the maximum dissipation($\rightarrow$ monotone scheme)
iii) Reduce or compensate the dissipation in the other parts of the flow.

We describe now two ways to implement this strategy.

2.1. *Flux limiter TVD method*

In the one-dimensional case, the coefficient of artificial viscosity d_e (related to an element) was evaluated using the variations of a sensor q over three contiguous elements. In the multidimensional case, we work with the segments and, using the extrapolated points $\{i*\}$ and $\{k*\}$, we construct the following variations :

$$\Delta_{i*}\, q \;=\; q_i - q_{i*} \;;\;\; \Delta_{ik}\, q \;=\; q_k - q_i \;;\;\; \Delta_{k*}\, q \;=\; q_{k*} - q_k$$

where q_{i*} and q_{k*} are determined by equations similar to Eq.(15) and Eq.(17). Denoting by r^+ and r^- the ratios :

$$r^+ = \frac{\Delta_{k*}\, q}{\Delta_{ik}\, q} \;\;;\;\; r^- = \frac{\Delta_{ik}\, q}{\Delta_{i*}\, q}$$

we define

$$d_{ik} = \begin{cases} 0 & \text{if } r^+ < 0 \text{ or } r^- < 0 \text{ (extremum)} \\ \text{1-B}(r_s^+, r_s^-) & \text{otherwise} \end{cases} \qquad (19)$$

where

$$r_s^+ = \frac{min(|\Delta_{ik}\, q|, |\Delta_{k*}\, q|)}{max(|\Delta_{ik}\, q|, |\Delta_{k*}\, q|)}$$

$$r_s^- = \frac{min(|\Delta_{i*}\, q|, |\Delta_{ik}\, q|)}{max(|\Delta_{i*}\, q|, |\Delta_{ik}\, q|)}$$

and $B(r_s^+, r_s^-) = min[B(r_s^+), B(r_s^-)]$.
The function $B(r)$ is a limiter function that takes values into the interval $[0,1]$. Some examples are

$$B(r) = min(\frac{2r}{1+r}, 1) \quad (\textit{ van Leer }) \tag{20}$$

$$B(r) = min(2r, 1) \quad (\textit{ Roe's superbee }) \tag{21}$$

Our own numerical experience indicates, that if the conservative variables are chosen as sensor, the solution presents oscillations in the non-conservative variables such as the pressure. A better choice is to take an unique sensor for the whole system of equations, so that the dissipation coefficient is the same for all the equations. In the examples illustrated later, the sensor is the Mach number ($M = \frac{\|\vec{w}\|}{c}$) which is a variable very sensitive to oscillations.

2.2. *Characteristic TVD method*

Another possibility is to work with characteristic variables. As a matter of fact, since system (1) is hyperbolic, any arbitrary linear combination of the Jacobian matrix A and B :

$$C = \eta_1 A + \eta_2 B$$

where η_1 and η_2 are real numbers, possess real eigenvalues : λ^1,λ^2,λ^3 and λ^4.
The right eigenvectors associated with the eigenvalues λ^l form the matrix T which diagonalises C, namely

$$T^{-1}CT = \Lambda \; ; \; \Lambda_{lj} = \lambda^l \delta_{lj}$$

The expressions of T and T^{-1} can be found in [5]. Let U_{ik} be some convenient average of U_i and U_k, and let λ^l_{ik}, T_{ik} denote the quantities λ^l, T evaluated at U_{ik} and where we have chosen η_1, η_2 as the components of the unit vector $\frac{\vec{\eta}}{\|\vec{\eta}\|}$. We define α_{ik} as the component of $\Delta_{ik}\, U_i$ in the lth characteristic direction, namely,

$$\Delta_{ik}\, U_i = T_{ik}\, \alpha_{ik} \; ; \; \alpha_{ik} = T_{ik}^{-1}\, \Delta_{ik}\, U_i \tag{22}$$

With the above notations, the artificial dissipation term can be written in the following form

$$D_{ik}\, U_i = T_{ik} \Psi_{ik} \tag{23}$$

where

$$\psi^l_{ik} = K_{ik}\, [\alpha^l_{ik} - \hat{Q}^l_{ik}] \tag{24}$$

and $\hat{Q}^l_{ik}$ is a limiter function.
Some examples of such a function are

$$\begin{aligned} (a) \quad & \hat{Q}^l_{ik} = minmod(\alpha^l_{i*}, \alpha^l_{ik}, \alpha^l_{k*}) \\ (b) \quad & \hat{Q}^l_{ik} = minmod(2\alpha^l_{i*}, 2\alpha^l_{ik}, 2\alpha^l_{k*}, \frac{1}{2}(\alpha^l_{i*} + \alpha^l_{k*})) \\ (c) \quad & \hat{Q}^l_{ik} = minmod(6\alpha^l_{i*}, \alpha^l_{ik}, 6\alpha^l_{k*}) \end{aligned} \tag{25}$$

The minmod function of a list of arguments is equal to the smallest number in absolute value if the arguments are of the same sign, or is equal to zero if any two arguments are of opposite sign.
Note that other ways to generalize TVD scheme in a finite element multidimensional context have been studid by Arminjon and Dervieux[6].

3. FCT methods

The basis of the Flux Corrected Transport (FCT) method or antidiffusion method is to use a modification of the diffusive scheme to remove the diffusion in the regular part of the flow and to limit it near discontinuities in such a way that no new maximum or minimum is formed. A method for constructing multidimensional FCT schemes has been proposed by Zalesak [7]. The following construction of a FCT finite element scheme is inspired from it.
Note that the relation between the first-order and second-order solutions can be expressed at node S_i in the form

$$MD_i \; u_i^H = MD_i \; u_i^L - \sum_k K_{ik}(u_k - u_i)$$

where u_i^H and u_i^L are the solution calculated by the second- and the first-order schemes respectively, and $MD_i \; u_i = \int_\Omega N_i u_i \; d\Omega$. Then, the procedure is as follows:

(1) Define for each segment the "antidiffusive flux"

$$at_{ik} = K_{ik}(u_k - u_i)$$

(2) Compute the update low order ("transported and diffused") solution :

$$u_i^{td} = u_i^L$$

(3) Limit the at_{ik} in such a manner that u^{n+1} as computed in the following step below is free of extrema not found in u^{td} and u^n :

$$at^c_{ik} = l_{ik} \; at_{ik} \; ; \; 0 \leq l_{ik} \leq 1$$

(4) Apply the limited antidiffusive fluxes :

$$MD_i\ u_i^{n+1} = MD_i\ u_i^{td} - \sum_k at_{ik}^c$$

Clearly for $l_{ik} = 1$ in step 3, the usual oscillatory solution would be obtained and so the selection of limiters is crucial to the properties of FCT. We restate here the FCT limiter presented in the paper of Zalesak.

For each node i, we define

$$P_i^+ = -\sum_k min(0,\ at_{ik})$$
$$Q_i^+ = MD_i\ (u_i^{max} - u_i^{td})$$
$$R_i^+ = \begin{cases} \min(1, Q_i^+/P_i^+) & \text{if } P_i^+ > 0 \\ 0 & \text{if } P_i^+ = 0 \end{cases}$$

and similarly

$$P_i^- = \sum_k max(0,\ at_{ik})$$
$$Q_i^- = MD_i\ (u_i^{td} - u_i^{min})$$
$$R_i^- = \begin{cases} \min(1, Q_i^-/P_i^-) & \text{if } P_i^- > 0 \\ 0 & \text{if } P_i^- = 0 \end{cases}$$

We have chosen the quantities l_{ik}, u_i^{max} and u_i^{min} as

$$l_{ik} = min(R_i^+, R_i^-, R_k^+, R_k^-)$$
$$u_i^{max} = max(u_i^a, u_{k1}^a, u_{k2}^a, ..., u_{km}^a)$$
$$u_i^{min} = min(u_i^b, u_{k1}^b, u_{k2}^b, ..., u_{km}^b)$$

where $S_{k1}, S_{k2}, ..., S_{km}$ represent the nodes surrounding node S_i, $u_i^a = max(u_i^n, u_i^{td})$ and $u_i^b = min(u_i^n, u_i^{td})$. But other choices are possible [6].

The correct method of limiting for a system of equations as the Euler equations is not obvious. We mention the choice

$$l_{ik} = min(l_{ik}^\rho, l_{ik}^{\rho u}, l_{ik}^{\rho v}, l_{ik}^e) \tag{26}$$

where l^ρ, $l^{\rho u}$, $l^{\rho v}$ and l^e are the limiters constructed for each conserved variable. We note that other finite element FCT schemes, using elemental contributions, have been proposed by Parrot and Christie [8], and by Morgan et al [9].

V. Numerical experiments

To illustrate the behaviour of the numerical schemes described in the previous section, an hypersonic flow around a blunt body is considered. The Mach number at infinity is 8.0, the angle of attack is zero and the initial condition is the uniform free-stream flow. The mesh contains 1908 nodes. We present plots of the following non dimensional numbers :

the pressure coefficient : $C_p = 2\dfrac{p - p_\infty}{\rho_\infty \| \vec{w}_\infty \|^2}$; the Mach number : $M = \dfrac{\| \vec{w} \|}{c}$;
the entropy deviation : $\Sigma = (p/p_\infty)/(\rho/\rho_\infty)^\gamma - 1$ and the non dimensional density : $Rho = (\rho/\rho_\infty) \ - 1$.

Our own experience indicates that the results obtained using the consistent mass matrix are qualitatively similar to those obtained with the lumped mass matrix when we reach the steady-state. Nevertheless, the oscillations are more rapidly damped in the first case; this behaviour has been already observed for one dimensional calculations. The inversion of mass matrix can be approximated by a purely explicit iterative technique of Jacobi type which takes a particulary simple form due to the incremental character of the scheme [2]. Only three iterations are needed to give a solution very close to those obtained with an exact technique.

Using the artificial viscosity method (Fig.2), we can obtain non oscillatory solutions. We note also the very good behaviour of the characteristic TVD scheme (Figs. 3-4), but the convergence depends of the limiter. In fact, if the convergence is very good for the limiter (25.b), it is harder for limiter (25.c) which is less dissipative. The flux limiter TVD scheme (Fig.5) gives the most dissipative results as can be seen on the curve of the entropy distribution along the body. The results obtained with the FCT scheme (Fig.6) gives monotonic profiles for the conservative variables, but it is not the case for non conservative variables such as pressure or velocity. Furthermore, the calculation do not converge. We can reduce the amplitude of the oscillations by adding artificial viscosity. Another solution would be perhaps to use characteristic variables in the limiting procedure.
We note that, for the illustrated results, the entropy jump at the shock is a little smaller than the theoretic value given in available shock tabulations.

We have also implemented a predictor-corrector version of the schemes of Richtmyer type [10,11]. The advantage of this algorithm is that it does not require the evaluation and subsequent multiplication of the Jacobian matrices A and B which

are very time-consuming. Using this scheme, the computational time is reduced by a factor 1.66 for the artificial viscosity method or the flux limiter TVD method, and by a factor 1.45 for the characteristic TVD method. The results obtained with the one-step and the predictor corrector approaches are very close. Nevertheless, the first one is a slightly more stable that the second one.
In all the calculations, we have used a local time stepping technique to accelerate the convergence.

VI. Future developments

1. Another first-order scheme

We have noted, in section III.2, that the first-order scheme can be interpreted as a second-order approximation of a parabolic equation of the form

$$\frac{\partial U}{\partial t} + \frac{\partial F}{\partial x} + \frac{\partial G}{\partial y} = \frac{h^2}{6\Delta t}\,\Delta U$$

where the coefficient of the diffusion term, i.e. $\frac{h^2}{6\Delta t}$, depends of the time increment in such a manner that the dissipative effect increases when the time increment decreases. This dependence can be removed if we replace the ratio $\frac{h}{\Delta t}$ by a quantity ω which has the dimension of a velocity. We propose the following first-order scheme in which the diffusion operator is constructed from the segments:

$$\int_\Omega N_i\, U_i^{n+1} d\Omega = \int_\Omega N_i\, U_i^n d\Omega + RH_i^n + \sum_k \frac{\omega_{ik}}{h_{ik}} K_{ik}^* (U_k^n - U_i^n) \qquad (27)$$

where $K_{ik}^* = 6K_{ik}$, h_{ik} is the size of the segment $\{ik\}$ and w_{ik} is the spectral radius of the matrix C on the segment $\{ik\}$, i.e.

$$\omega_{ik} = |\eta_1 u_{ik} + \eta_2 v_{ik}| + c_{ik}$$

The Mach-8 calculations obtained with the first-order schemes (5) and (27) are illustrated in Figs. 7 and 8, respectively. The numerical solutions are very similar for the two schemes. Moreover, the new first-order scheme seems to be a little less dissipative than the old one. Experiments using the artificial viscosity method (Figs. 9 and 10) show that the entropy jump is better represented when we use the new scheme, for which the artificial viscosity term does not depend anymore of the time increment. This might be important when the solution reaches the steady-state.

2. Multistage time stepping scheme

Multistage schemes for the numerical solution of ordinary differential equations are usually designed to give a high order of accuracy. In these schemes, Eqs.(1) are first discretized in space, so as to get a set of ordinary differential equations which can be solved subsequently by a Runge-Kutta method.
The spatial discretization of Eq.(1) can be written as

$$\int_\Omega N_i \frac{\partial U}{\partial t} d\Omega = Q_i \tag{28}$$

where

$$Q_i = \int_\Omega [\frac{\partial N_i}{\partial x} F + \frac{\partial N_i}{\partial y} G] d\Omega - \int_\Gamma N_i [F\kappa_x + G\kappa_y] d\Gamma$$

For simplification, we diagonalize the consistent mass matrix. Thus, Eq.(28) becomes

$$\frac{\partial U_i}{\partial t} = \frac{1}{MD_i} Q_i \tag{29}$$

where $MD_i = \int_\Omega N_i d\Omega$. Finally, if we add an artificial viscosity term, Eq.(29) can be rewritten as

$$\frac{\partial U_i}{\partial t} = R_i \tag{30}$$

in which

$$R_i = \frac{1}{MD_i}(Q_i + D_i)$$

and where D_i is a diffusion operator constructed as in (10) or (27).

Let U^n be the value of U after n time steps. The general m stage scheme to advance a time step Δt can be written as

$$\begin{aligned} U^{(0)} &= U^n \\ U^{(1)} &= U^{(0)} + \beta_1 \Delta t \; R^{(0)} \\ \ldots &= \ldots \\ U^{(m-1)} &= U^{(0)} + \beta_{m-1} \Delta t \; R^{(m-2)} \\ U^{(m)} &= U^{(0)} + \beta_m \Delta t \; R^{(m-1)} \\ U^{n+1} &= U^{(m)} \end{aligned} \tag{31}$$

An efficient 4 stage scheme, which is also fourth order accurate for linear problems, can be construct with the coefficients :

$$\beta_1 = \frac{1}{4} \; ; \; \beta_2 = \frac{1}{3} \; ; \; \beta_3 = \frac{1}{2} \; ; \; \beta_4 = 1 \quad .$$

VII. Conclusion

In this report, we have presented different techniques to construct second-order shock-capturing schemes in a finite element multidimensional context. The artificial viscosity method appears to be the least diffusive in the regular part of the flow but introduces a parameter which is problem dependent. On the other hand, TVD and FCT methods have not this disadvantage but the quality of the solution depends on the limiter function. Moreover, these schemes sometimes add dissipation in the smooth region of the flow. For steady-state calculations, we have observed that the calculations always converge when the artificial viscosity method is used but not always for the other methods. In fact, the convergence is greatly influenced by the type of limiter functions.

The first-order scheme employed here has a dissipative effect which depends on the time step. This dependence can be removed by multiplying the artificial viscosity term by an appropriate 'Courant number'. Moreover, the schemes are of Lax-Wendroff type, in the sense that steady-state solutions depend on the value of the time step. At present time, we investigate multistage time stepping versions of the schemes. Another way of ameliorating the schemes is perhaps to use an upwind scheme as first-order scheme. Nevertheless, these schemes are much less dissipative than the centered first-order ones.
Finally, using the concept of segments, the previous schemes can be easily generalized for three-dimensional calculations with tetrahedra.

ACKNOWLEDGEMENTS

The author would like to take this opportunity to acknowledge many fruitful and stimulating discussions during the course of the present work with Professor Alain Dervieux.

VIII. References

[1] V. SELMIN, Finite Element Solution of Hyperbolic Equations. I.One Dimensional Case; INRIA Research Report 655 (1987) .

[2] J. DONEA, A Taylor-Galerkin Method for Convective Transport Problems; Internat. J. Numer. Methds. Engrg. 20(1984) 101-120 .

[3] P.D. LAX and B. WENDROFF, Difference Schemes for Hyperbolic Equations with High Order of Accuracy; Comm. Pure Appl. Math. 17(1964) .

[4] J. DONEA, L. QUARTAPELLE and V. SELMIN, An Analysis of Time Discretization in the Finite Element Solution of Hyperbolic Problems; J. Comput. Phys. 70(1987), 463-499 .

[5] G. VIJAYASUNDARAM, Résolution numérique des équations d' Euler pour des écoulements transsoniques avec un schéma de Godunov en Eléments Finis; Thesis, University Paris VI (1983) .

[6] P. ARMINJON and A. DERVIEUX, ; INRIA Research Report in preparation .

[7] S.T. ZALESAK, Fully Multidimensional Flux-Corrected Transport Algorithms for Fluids; J. Comput. Phys. 31(1979) 335-362 .

[8] A.K. PARROTT and M.A. CHRISTIE, FCT Applied to the 2-D Finite Element Solution of Tracer Transport by a Single Phase Flow in a Porous Medium; in Proc of the ICFD Conference on Numerical Methods for Fluid Dynamics, Reading, April 1985 .

[9] K. MORGAN, R. LOEHNER, J.R. JONES, J. PERAIRE and M. VAHDATI, Finite Element FCT for the Euler and Navier-Stokes Equations; in Proc. 6th Int. Symp. Finite Element Methods in Flow Problems, INRIA (1986) .

[10] F. ANGRAND, A. DERVIEUX, V. BOULARD, J. PERIAUX and G. VIJAYASUNDARAM; Transonic Euler Simulations by Means of Finite Element Explicit Schemes, AIAA Paper 83-1924 .

[11] R. LOEHNER, K. MORGAN and O.C. ZIENKIEWICZ; An Adaptative Finite Element Procedure for High Speed Flows, Comp. Meth. Appl. Mech. Engrg. 51, 441-465(1985) .

Artificial viscosity method
Sensor : second derivative of the pressure
Consistent mass matrix ; CFL=0.6 ; $\chi = 2.0$

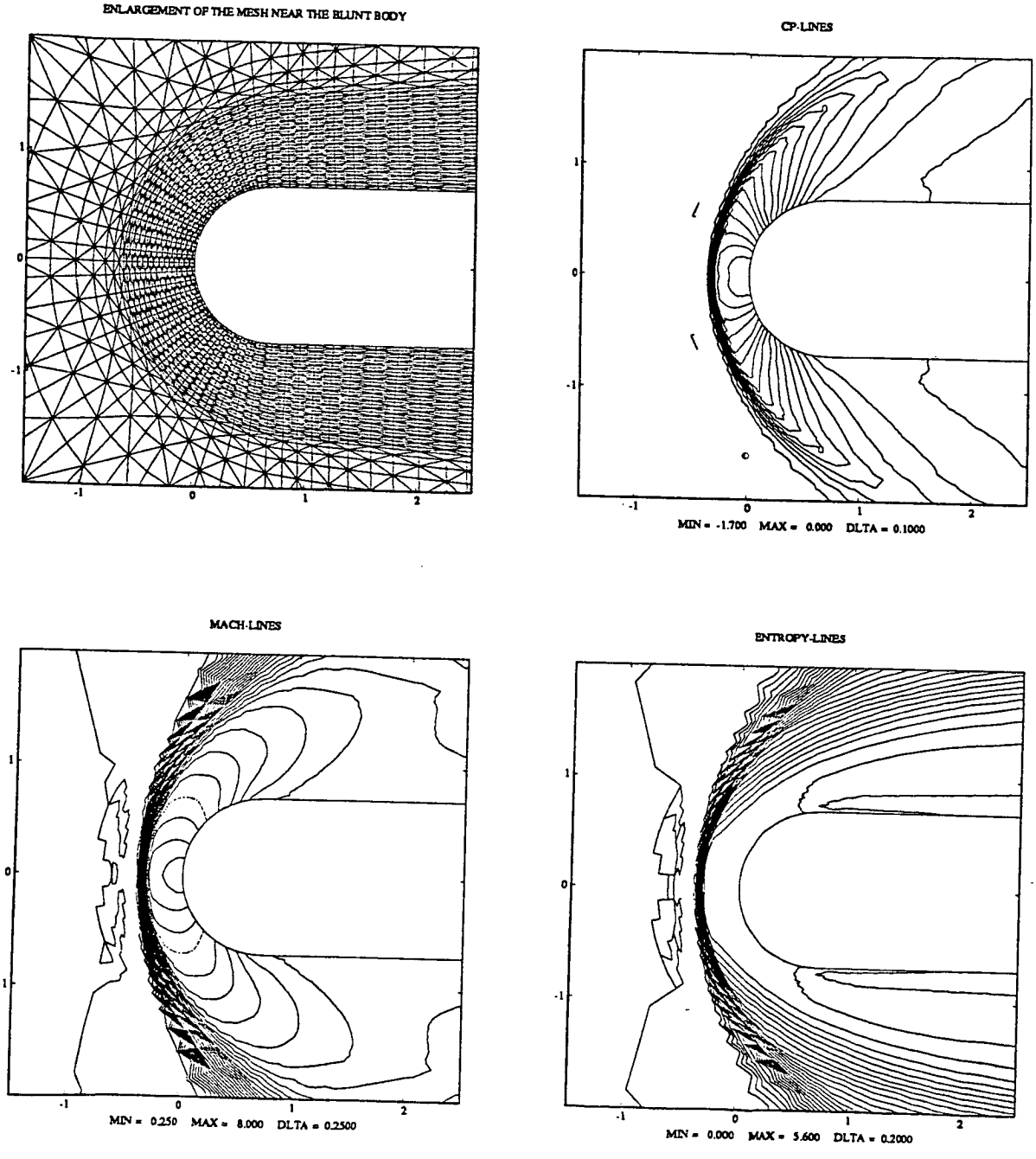

Fig. 2 : Artificial viscosity method

Artificial viscosity method
Sensor : second derivative of the pressure
Consistent mass matrix ; CFL=0.6 ; $\chi = 2.0$

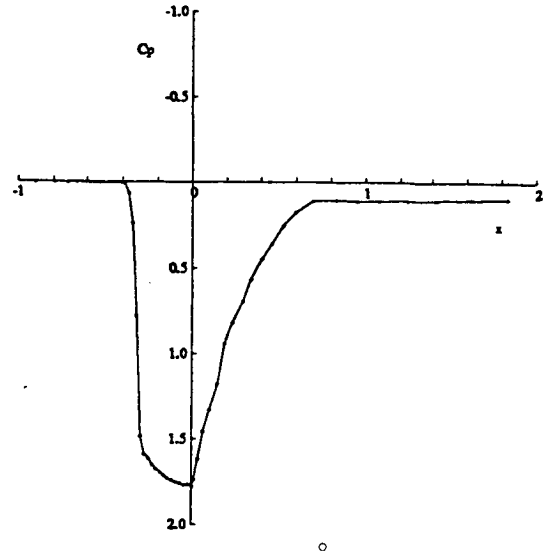

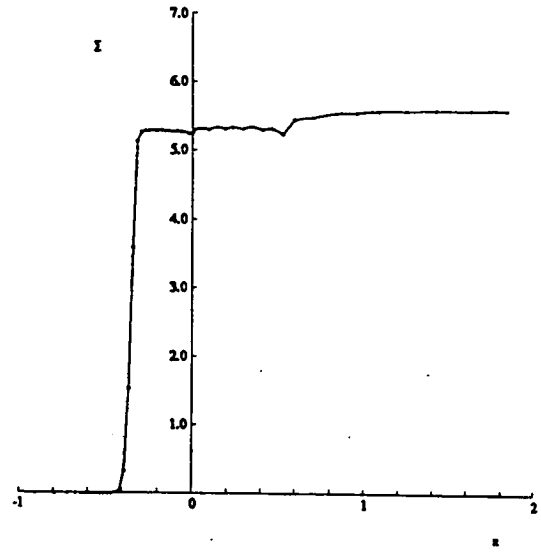

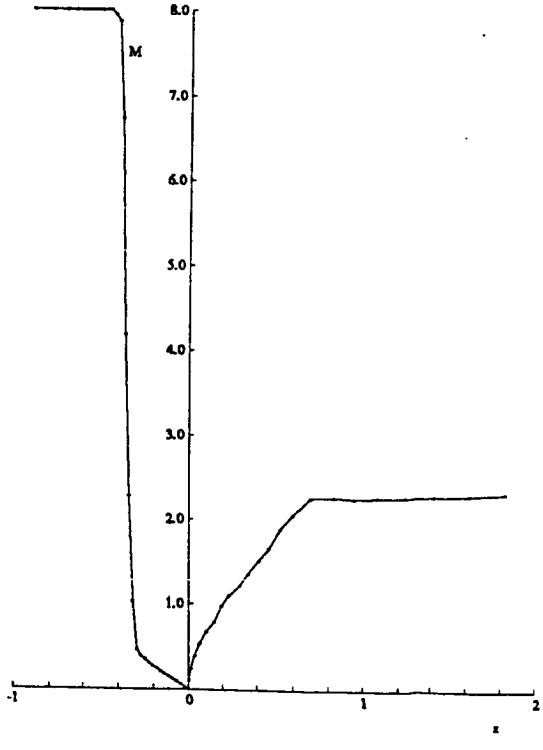

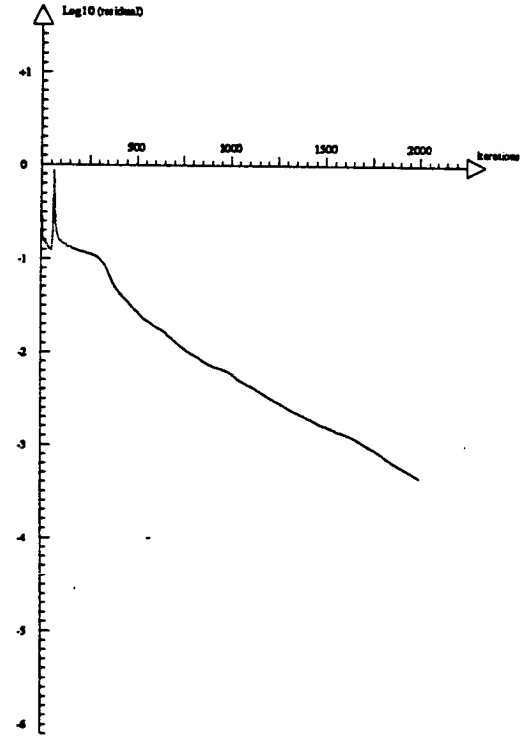

Fig. 2 : Continued

Characteristic TVD scheme (2-s)
Limiter two
Consistent mass matrix ; CFL=0.8

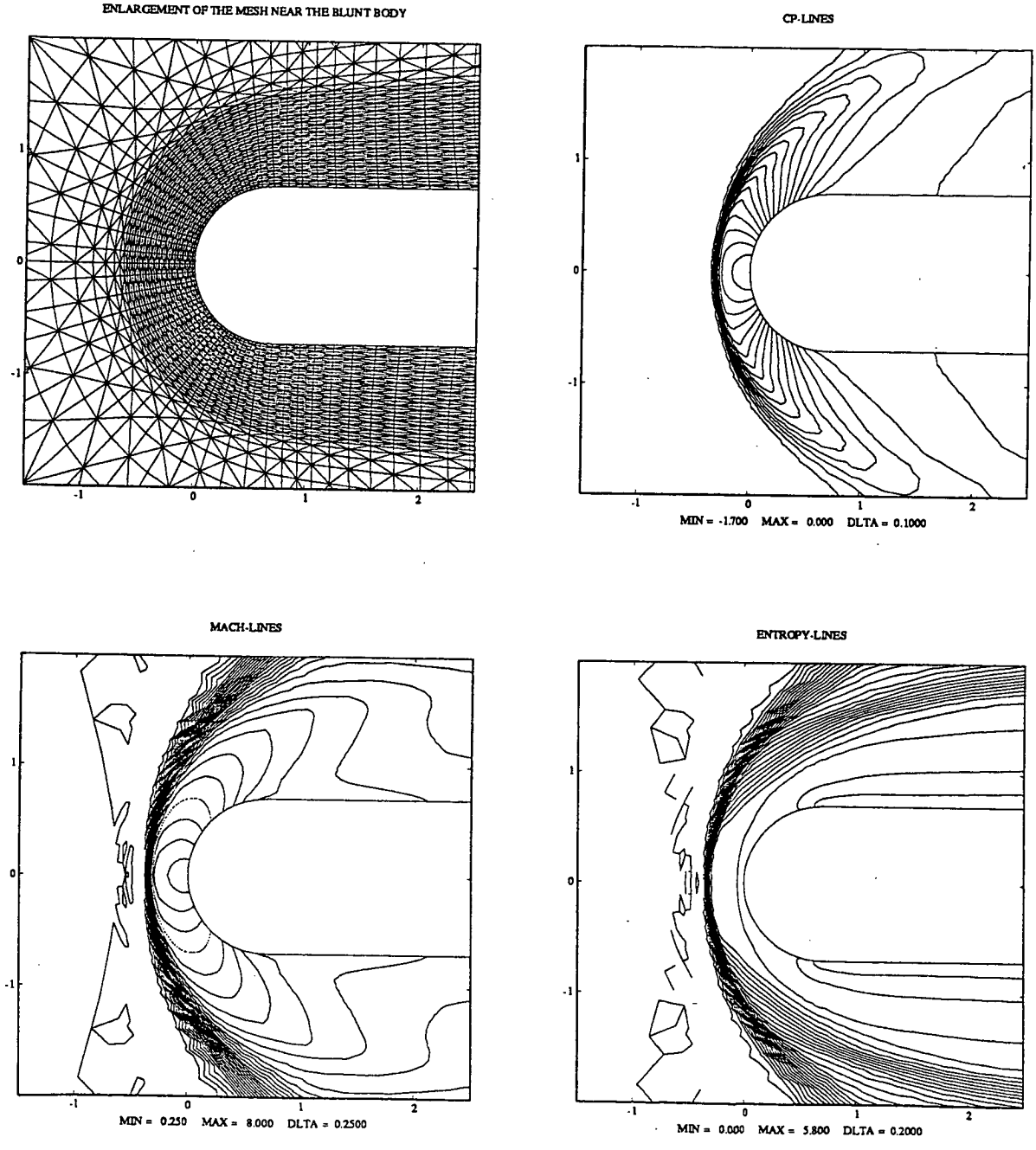

Fig. 3 : Characteristic TVD method, limiter 25.b

Characteristic TVD scheme (2-s)
Limiter two
Consistent mass matrix ; CFL=0.8

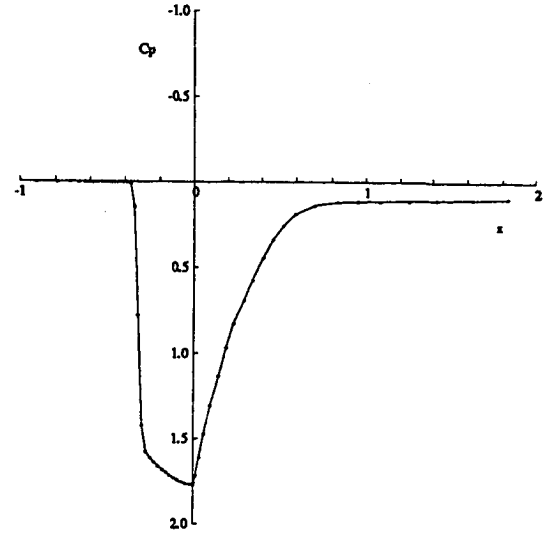

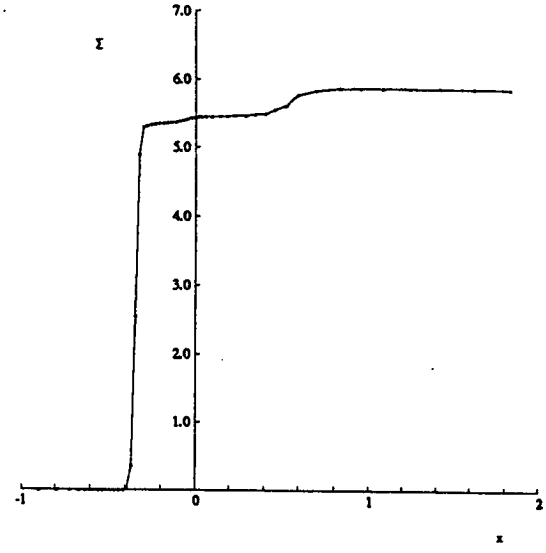

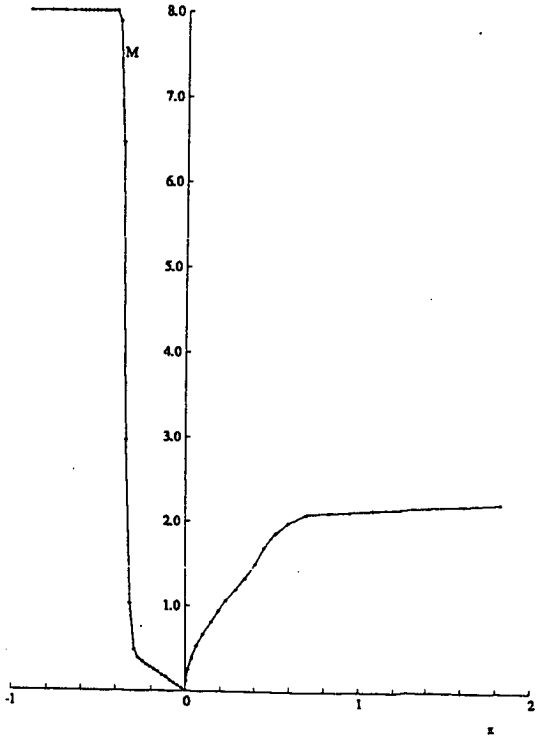

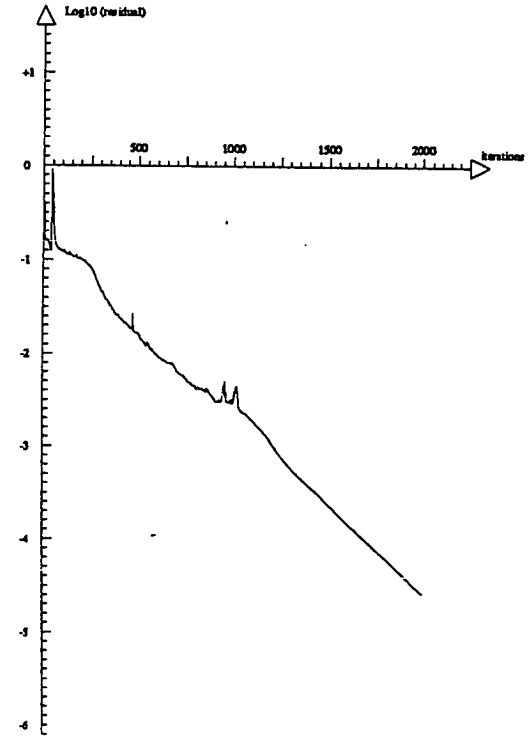

Fig. 3 : Continued

Characteristic TVD scheme(2-s)
Limiter three
Consistent mass matrix ; CFL=0.5

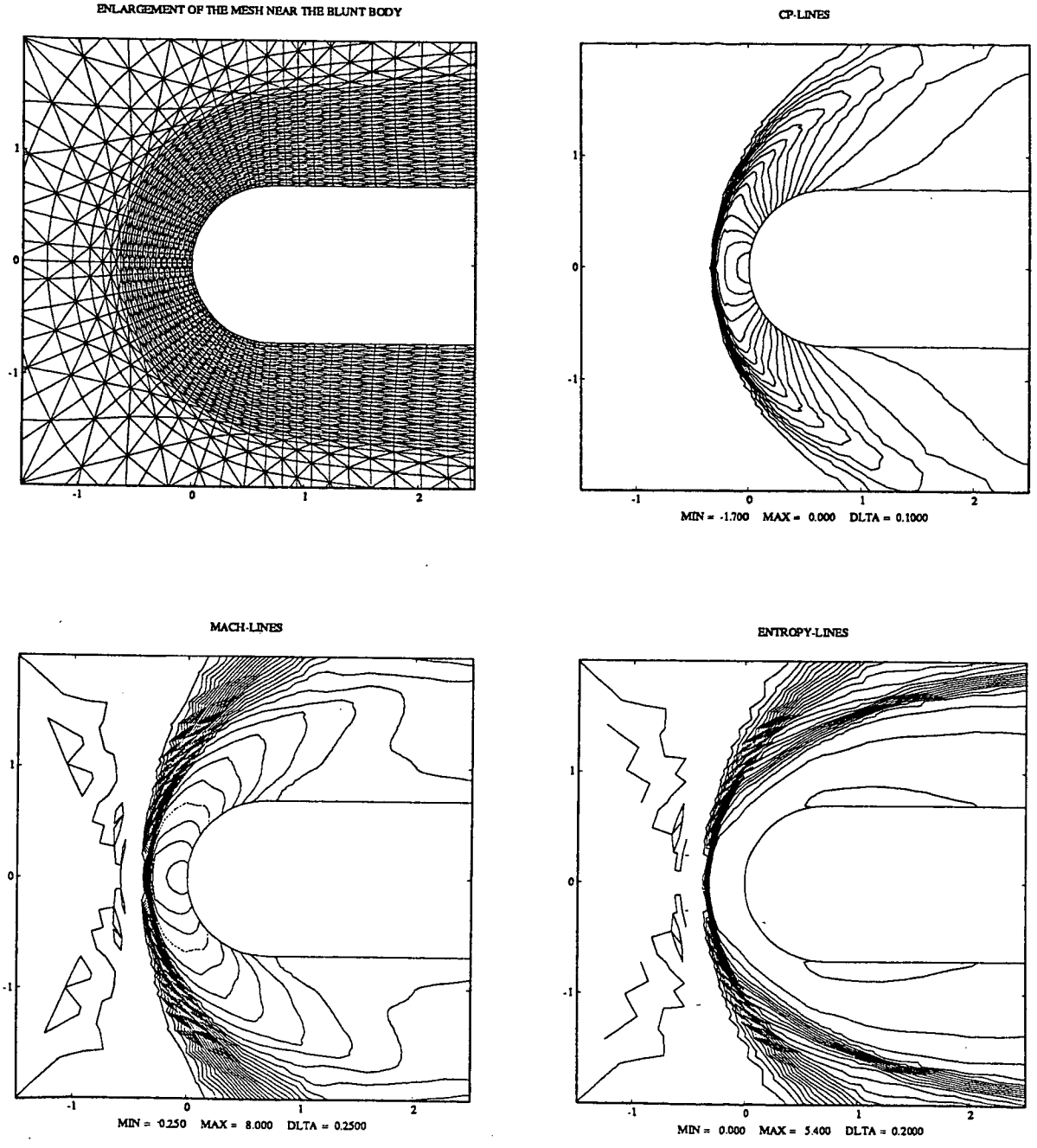

Fig. 4 : Characteristic TVD method, limiter 25.c

Characteristic TVD scheme(2-s)
Limiter three
Consistent mass matrix ; CFL=0.5

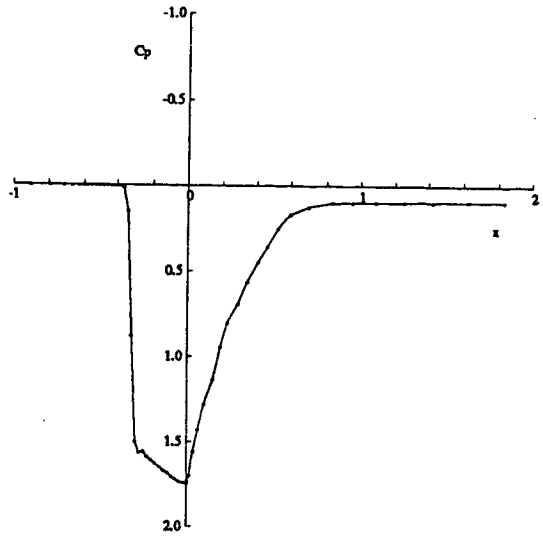

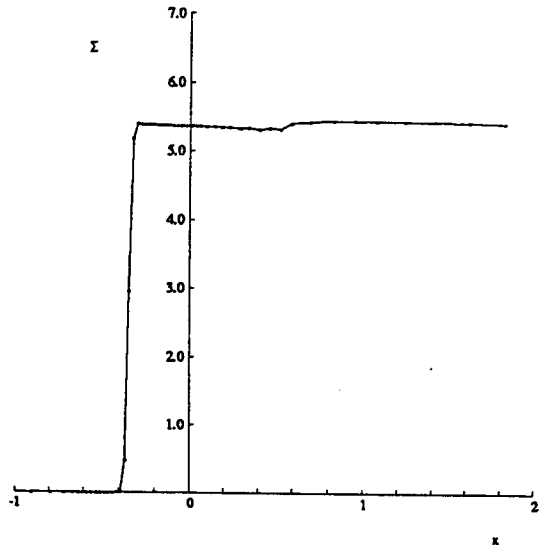

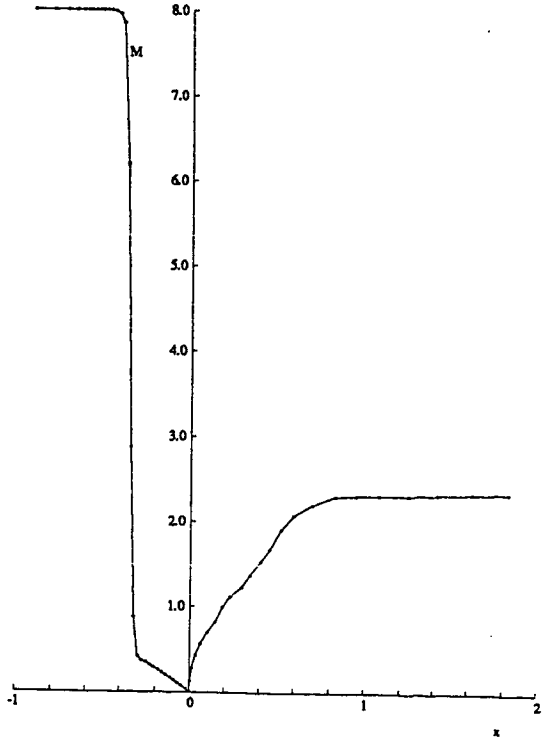

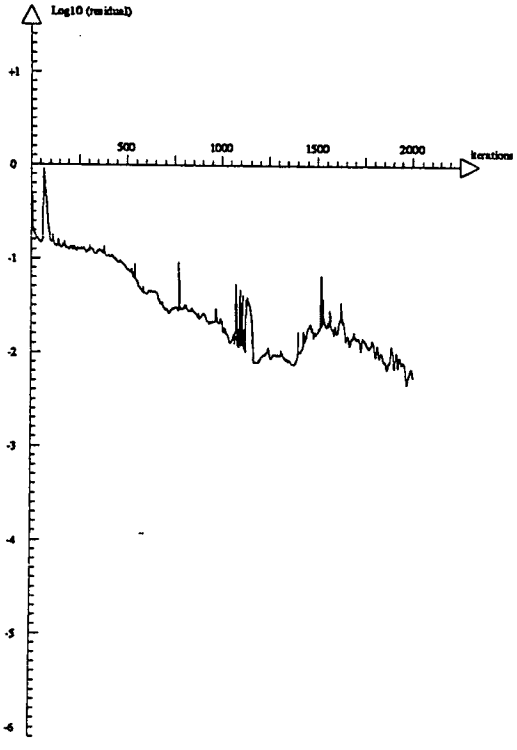

Fig. 4 : Continued

Flux Limiter TVD scheme (2-s)
Limiter : Roe's superbee
Consistent mass matrix ; CFL=0.5

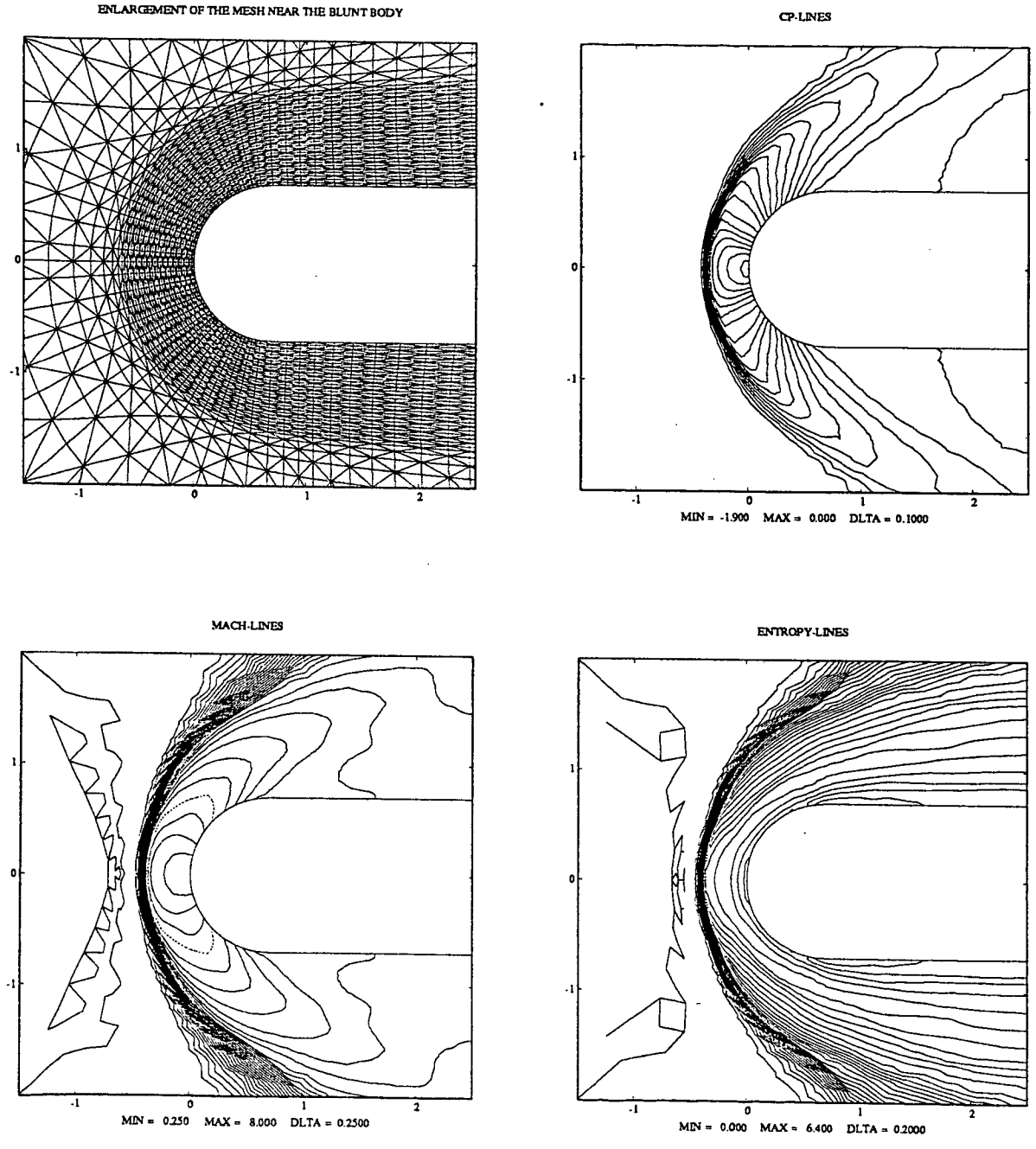

Fig. 5 : Flux limiter TVD method

Flux Limiter TVD scheme (2-s)
Limiter : Roe's superbee
Consistent mass matrix ; CFL=0.5

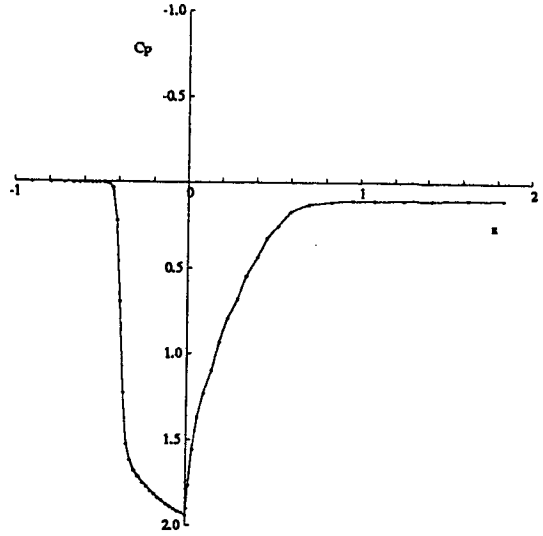

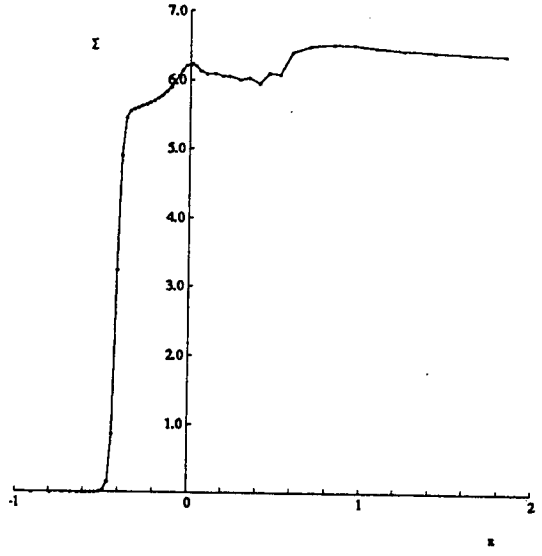

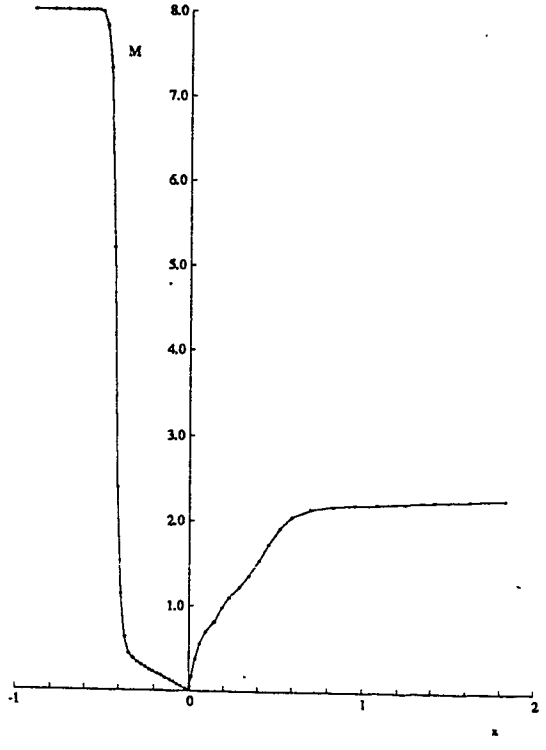

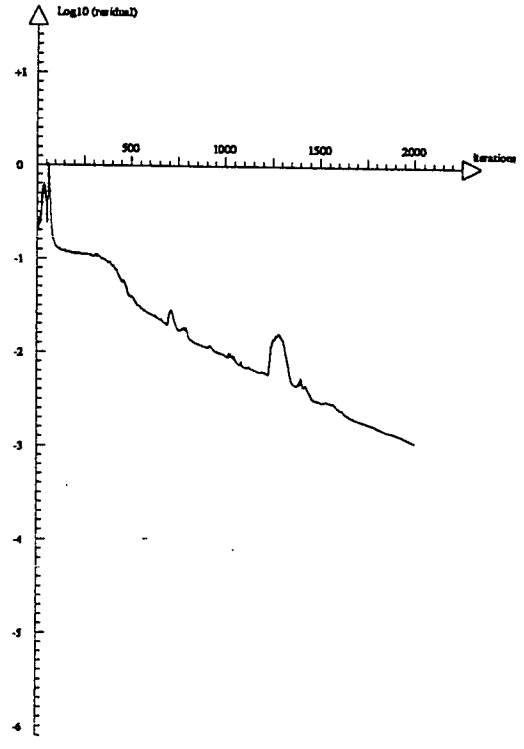

Fig. 5 : Continued

FCT scheme (2-s)
Limiter : $min(l^\rho, l^m, l^n, l^e)$
Consistent mass matrix ; CFL=0.5

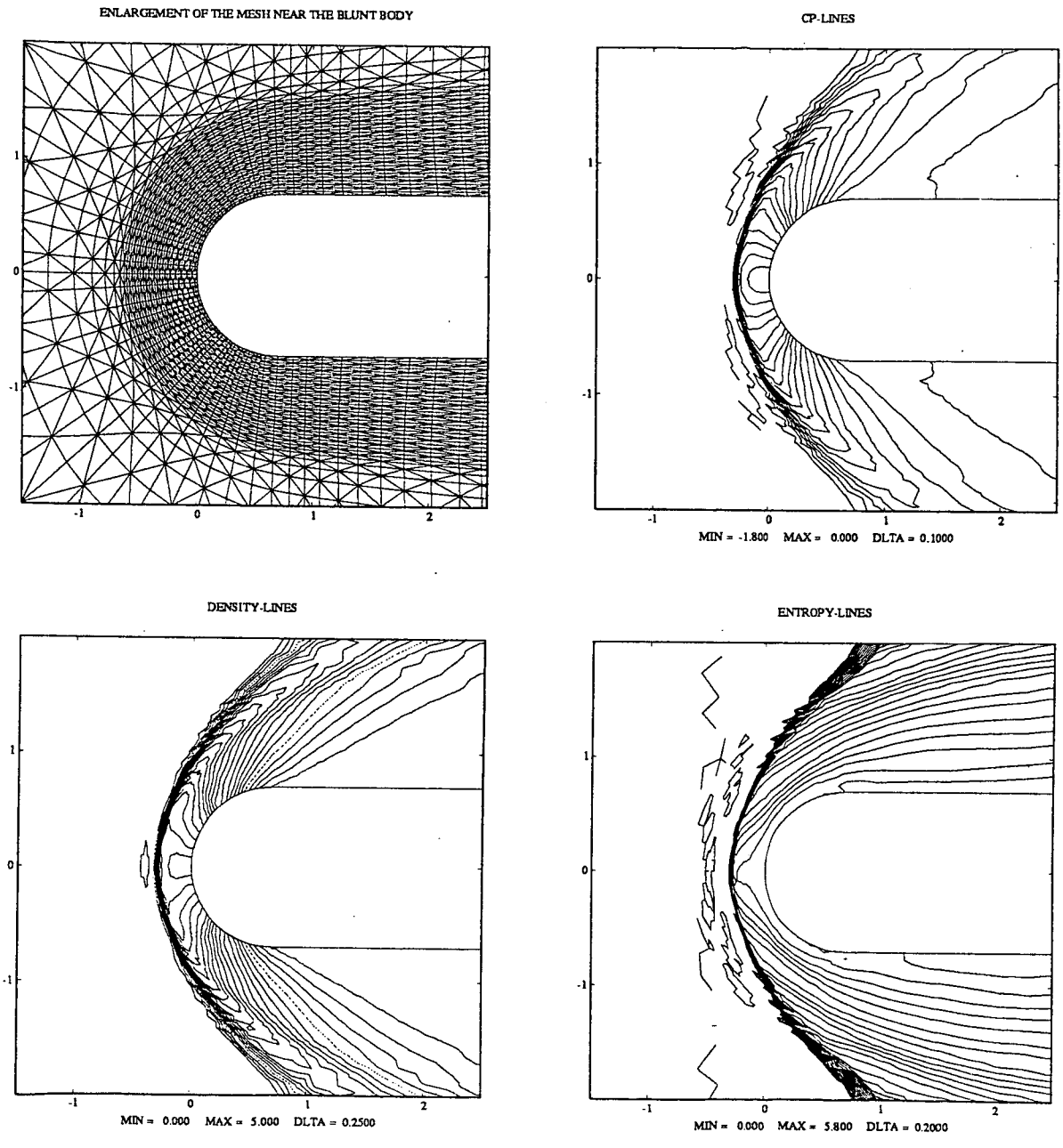

Fig. 6 : FCT method

FCT scheme (2-s)
Limiter : $min(l^\rho, l^m, l^n, l^e)$
Consistent mass matrix ; CFL=0.5

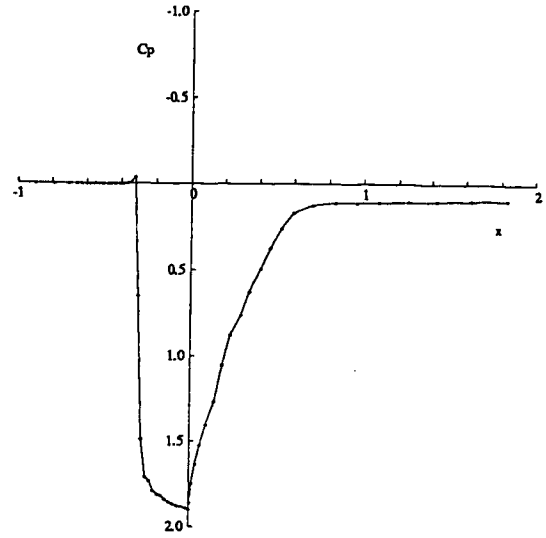

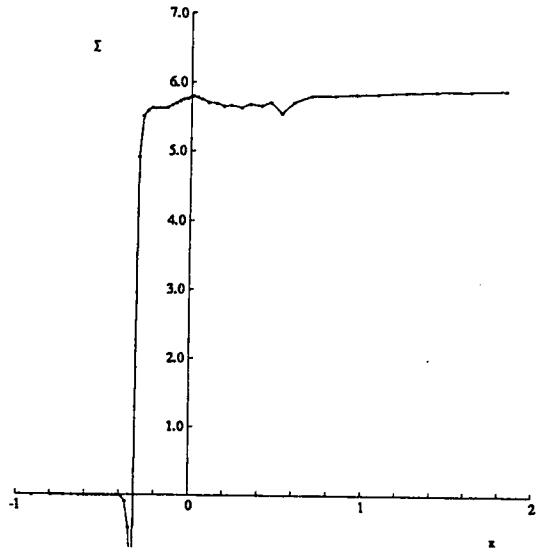

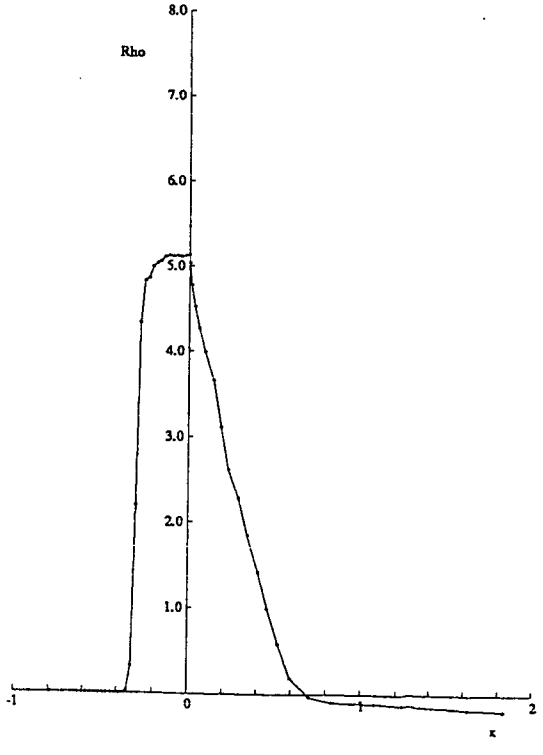

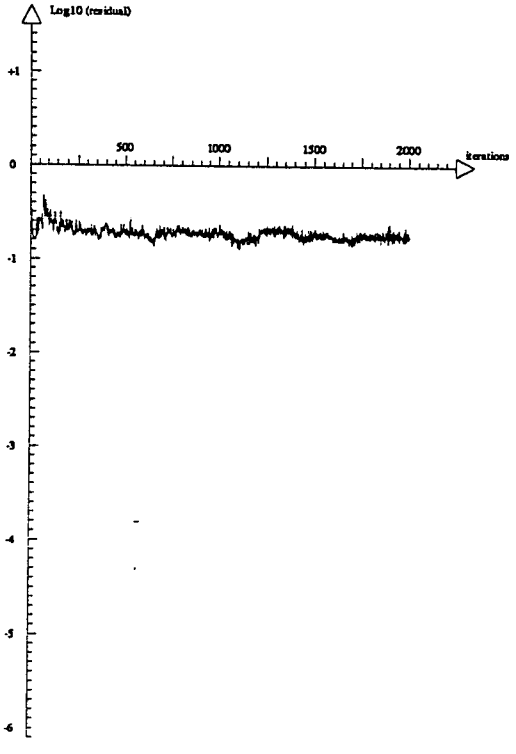

Fig. 6 : Continued

First-order scheme (2-s)
with time increment dependence of the viscosity
CFL=0.5

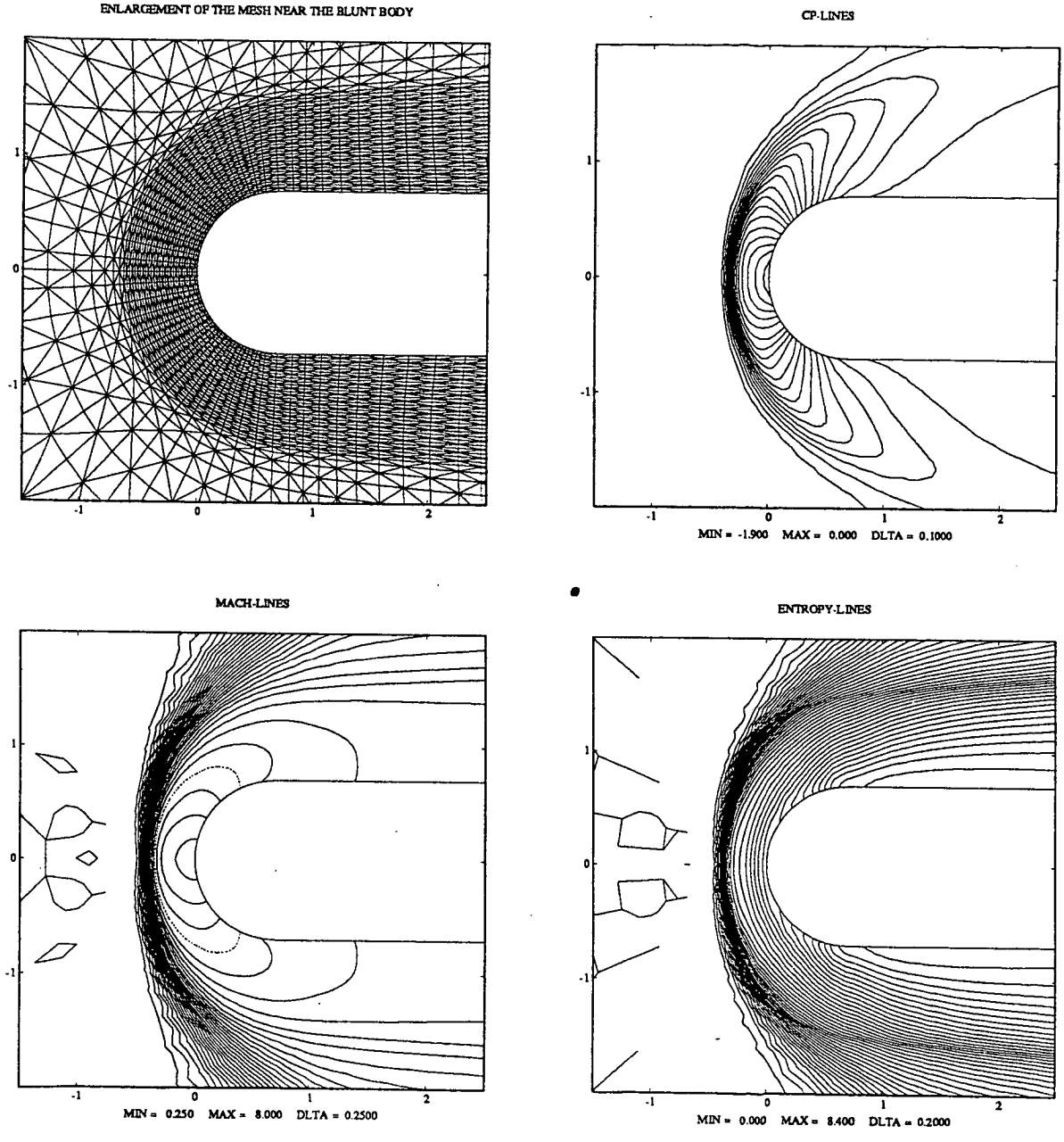

Fig. 7 : First-order scheme

First-order scheme (2-s)
with time increment dependence of the viscosity
CFL=0.5

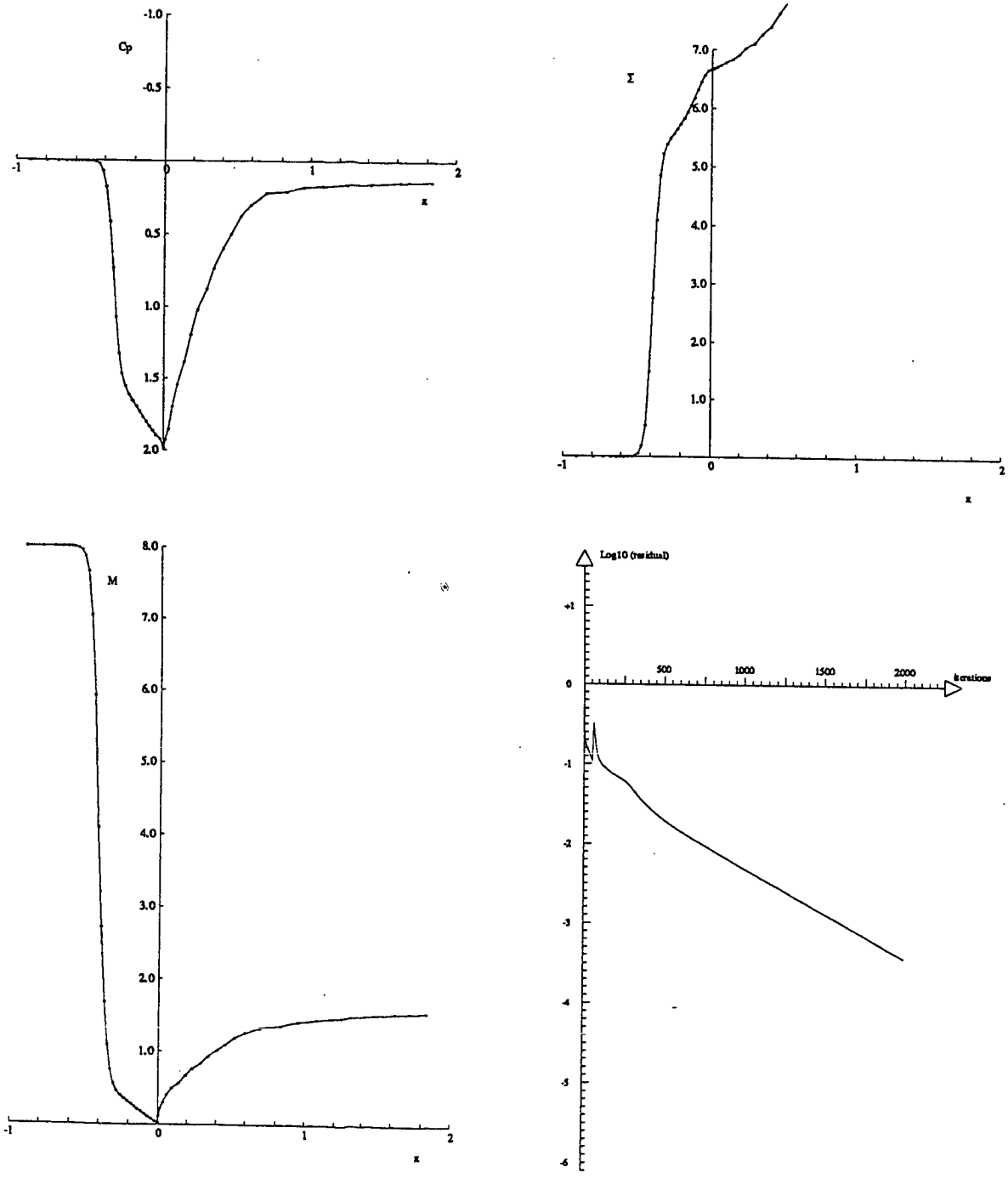

Fig. 7 : Continued

First-order scheme (2-s)
with eigenvalue dependence of the viscosity
CFL=0.5

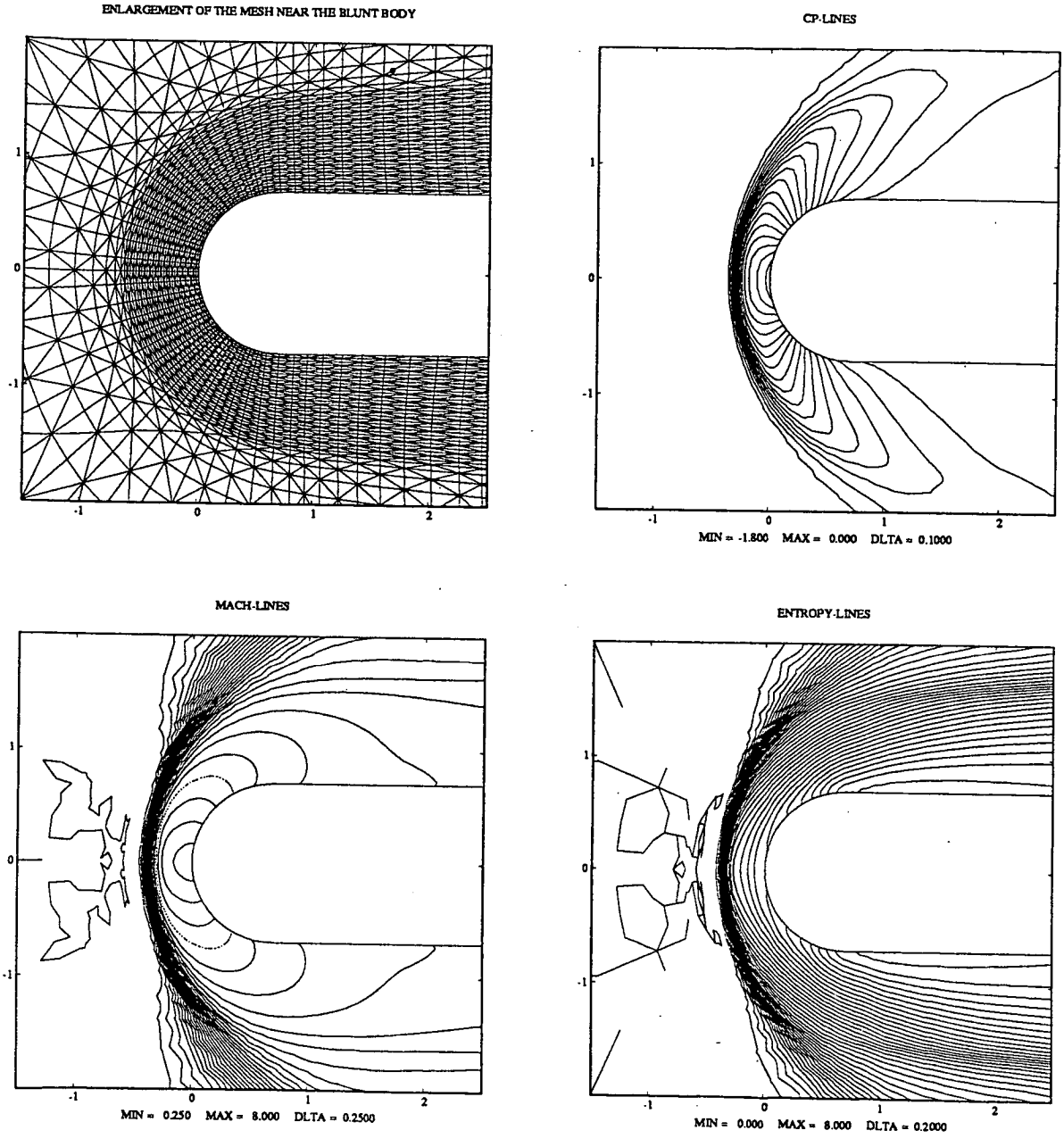

Fig. 8 : First-order scheme

First-order scheme (2-s)
with eigenvalue dependence of the viscosity
CFL=0.5

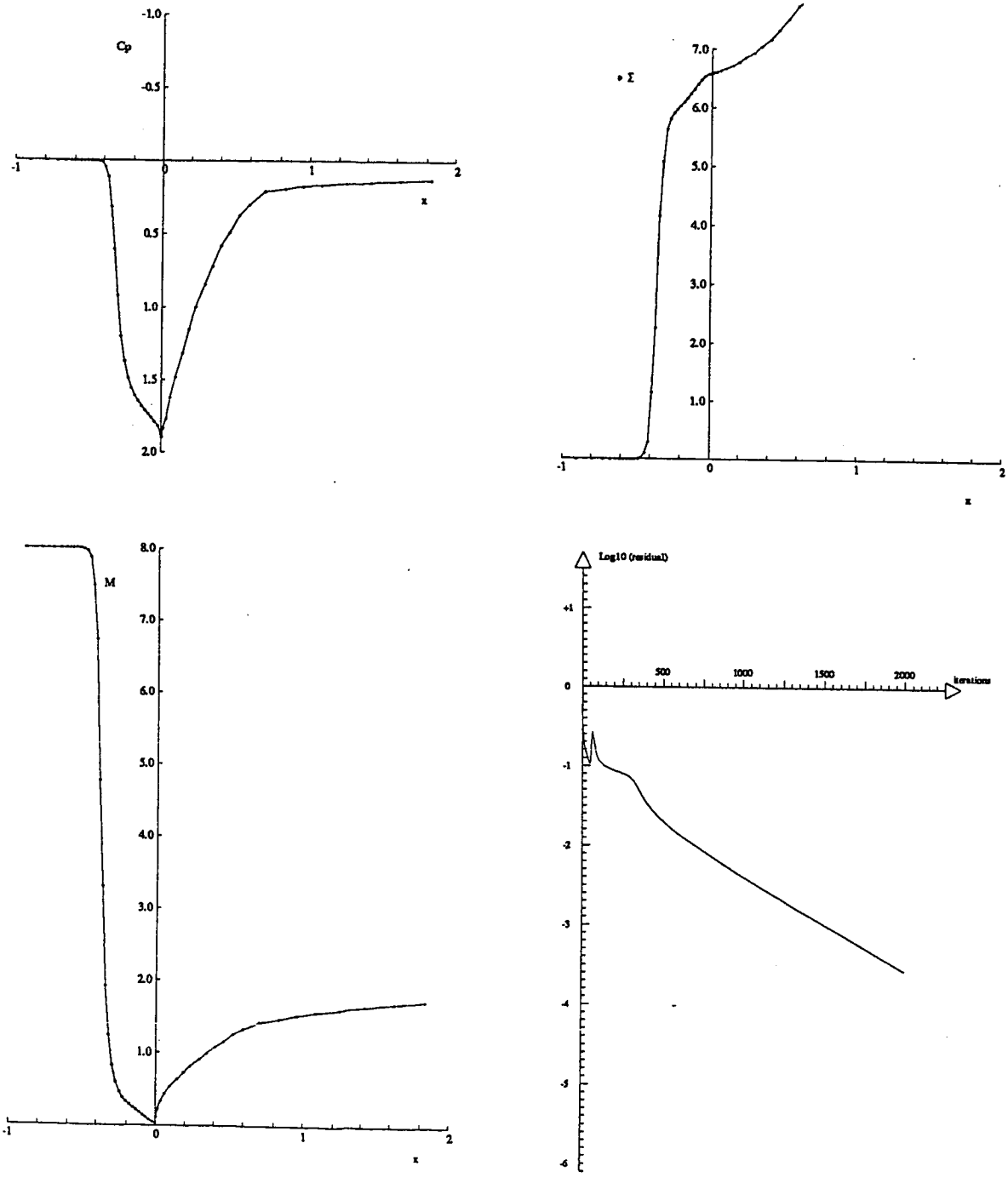

Fig. 8 : Continued

Artificial viscosity method (2-s)
Sensor : second derivative of the pressure
Lumped mass matrix ; CFL=0.5 ; χ=2.0

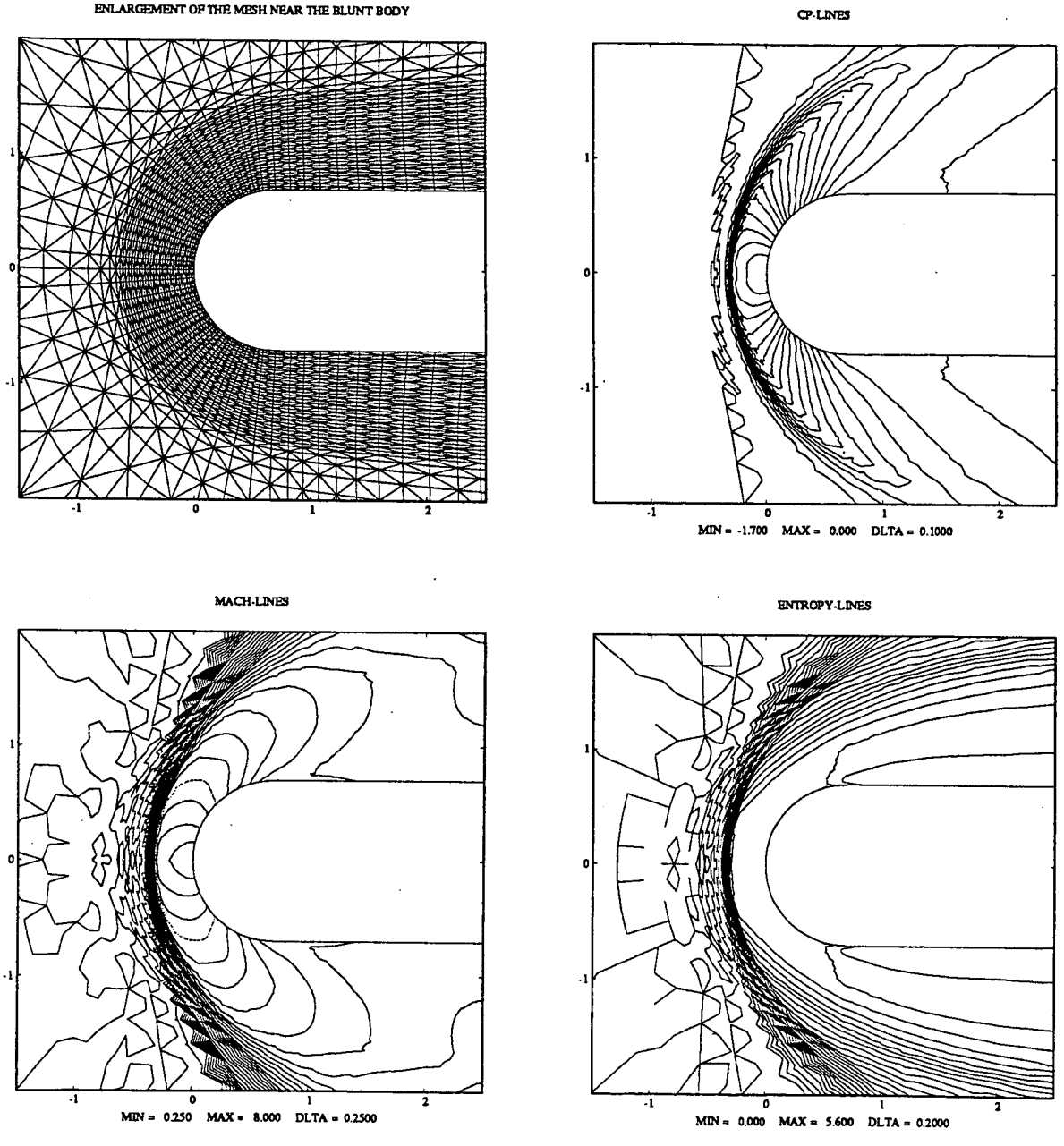

Fig. 9 : Artificial viscosity method

Artificial viscosity method (2-s)
Sensor : second derivative of the pressure
Lumped mass matrix ; CFL=0.5 ; χ=2.0

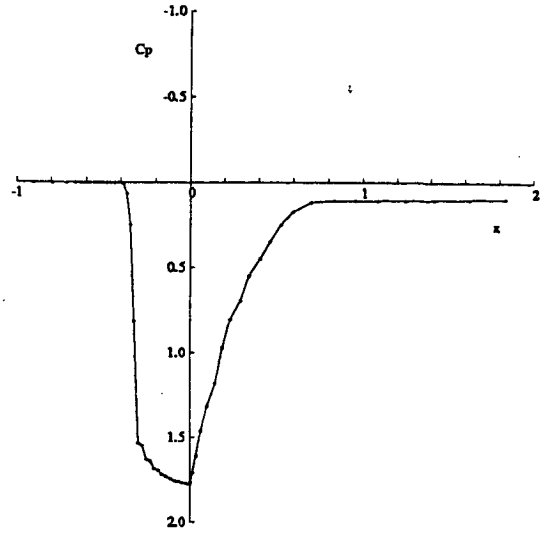

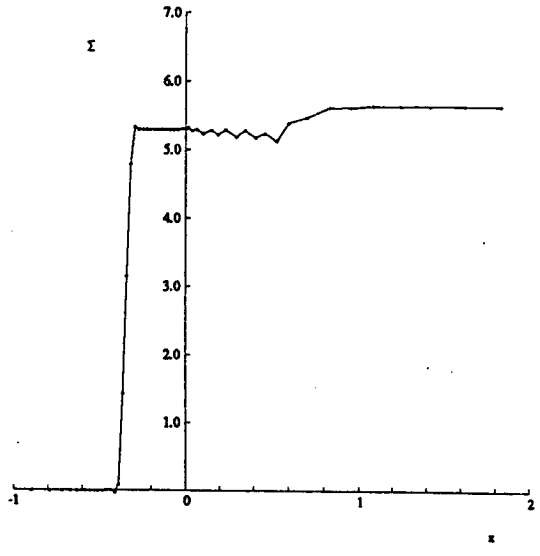

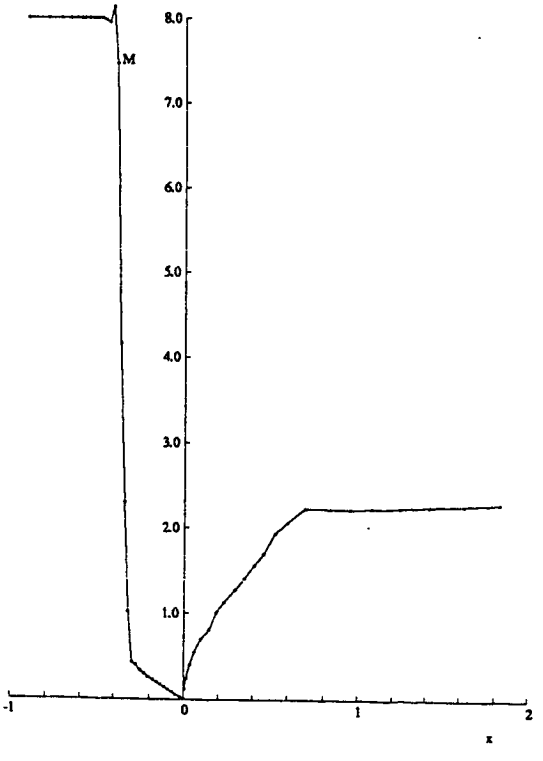

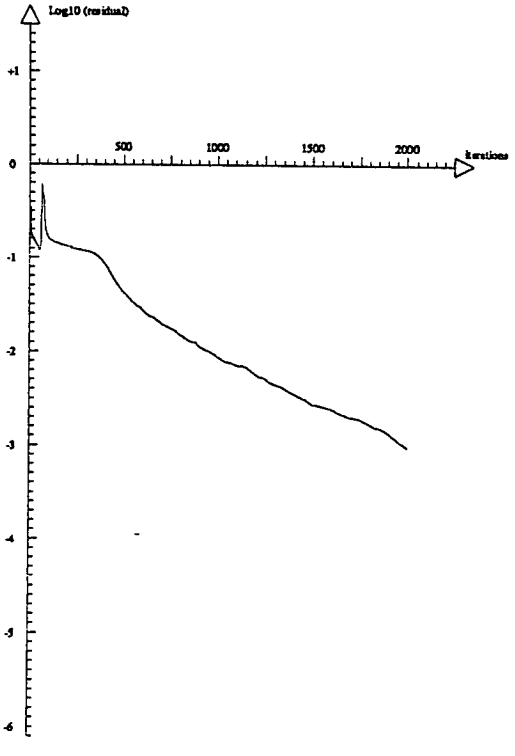

Fig. 9 : Continued

Artificial viscosity method (2-s)
with eigenvalue dependence of the viscosity
Sensor : second derivative of the pressure
CFL=0.5 ; χ=2.0

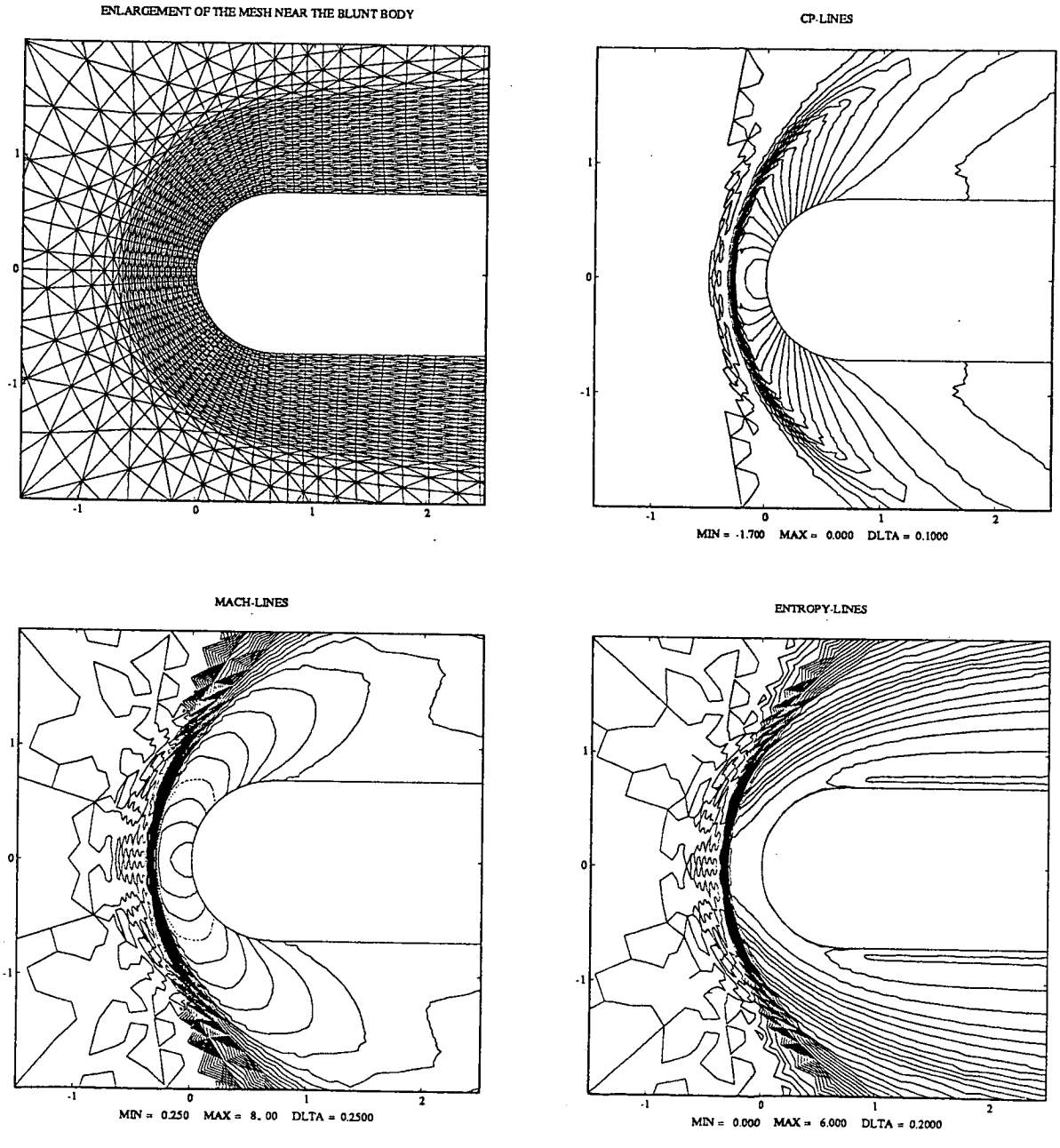

Fig.10 : Artificial viscosity method

Artificial viscosity method (2-s)
with eigenvalue dependence of the viscosity
Sensor : second derivative of the pressure
CFL=0.5 ; χ=2.0

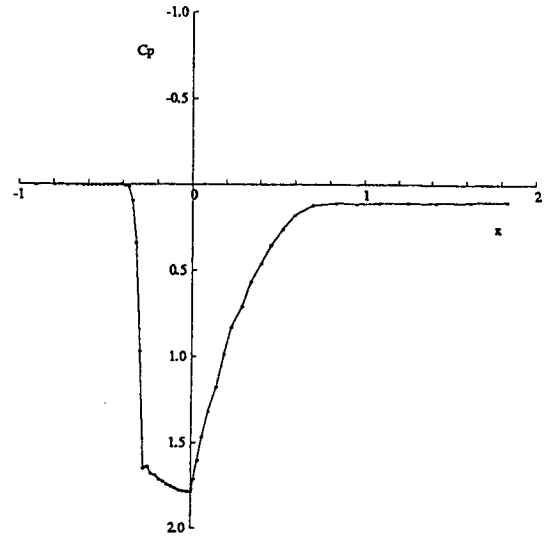

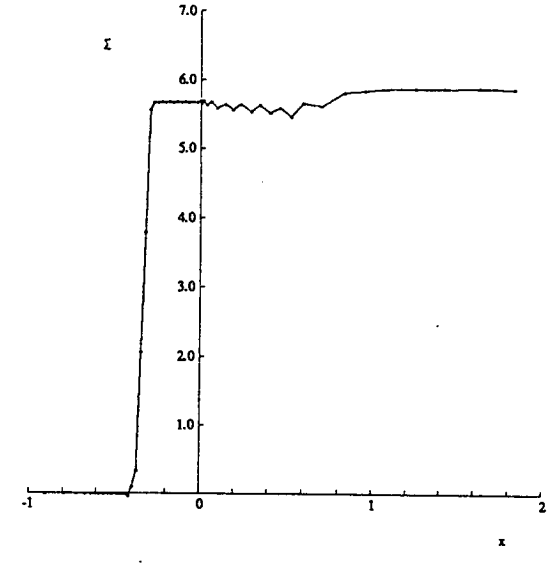

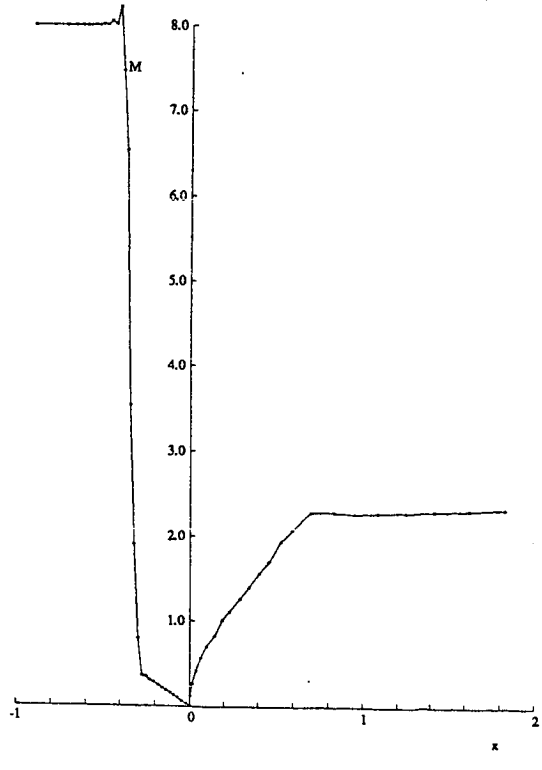

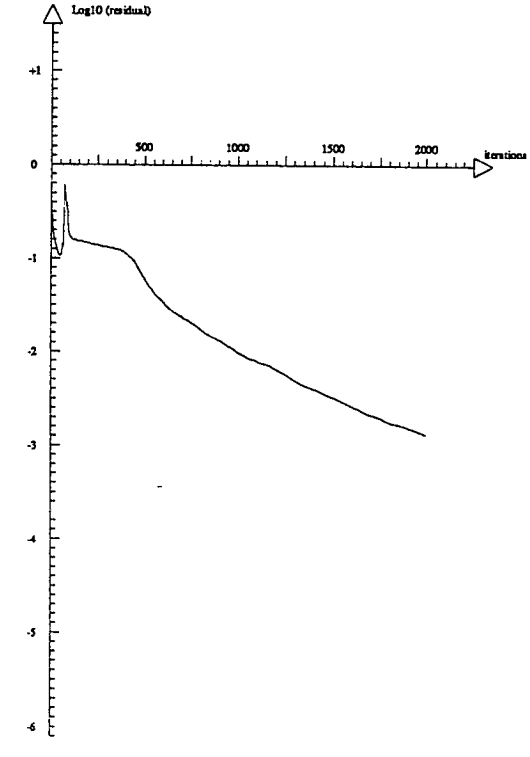

Fig.10 : Continued

Imprimé en France
par
l'Institut National de Recherche en Informatique et en Automatique